Giant Planets

Tristan Guillot, Daniel Gautier

Available online at www.sciencedirect.com

ScienceDirect

Treatise on Geophysics, 2nd Edition 00 (2014) 1–41

To appear in Treatise on Geophysics, 2nd Edition, Eds. T. Spohn & G. Schubert

Giant Planets

Tristan Guillot[a,*], Daniel Gautier[b]

[a] *Laboratoire Lagrange, Université de Nice-Sophia Antipolis, Observatoire de la Côte d'Azur, CNRS, CP 34229, 06304 NICE Cedex 04, France*
[b] *LESIA, Observatoire de Paris, CNRS FRE 2461, 5 pl. J. Janssen, 92195 Meudon Cedex, France*

Abstract

We review the interior structure and evolution of Jupiter, Saturn, Uranus and Neptune, and giant exoplanets with particular emphasis on constraining their global composition. Compared to the first edition of this review, we provide a new discussion of the atmospheric compositions of the solar system giant planets, we discuss the discovery of oscillations of Jupiter and Saturn, the significant improvements in our understanding of the behavior of material at high pressures and the consequences for interior and evolution models. We place the giant planets in our Solar System in context with the trends seen for exoplanets.

Keywords: Giant planets, exoplanets, Jupiter, Saturn, Uranus, Neptune, planet formation

*Corresponding author
Email address: tristan.guillot@oca.eu (Tristan Guillot)

Contents

1. Introduction

In our solar system, four planets stand out for their sheer mass and size. Jupiter, Saturn, Uranus, and Neptune indeed qualify as "giant planets" because they are larger than any terrestrial planet and much more massive than all other objects in the solar system, except the Sun, put together (Figure 1). Because of their gravitational might, they have played a key role in the formation of the solar system, tossing around many objects in the system, preventing the formation of a planet in what is now the asteroid belt, and directly leading to the formation of the Kuiper Belt and Oort Cloud. They also retain some of the gas (in particular hydrogen and helium) that was present when the Sun and its planets formed and are thus key witnesses in the search for our origins.

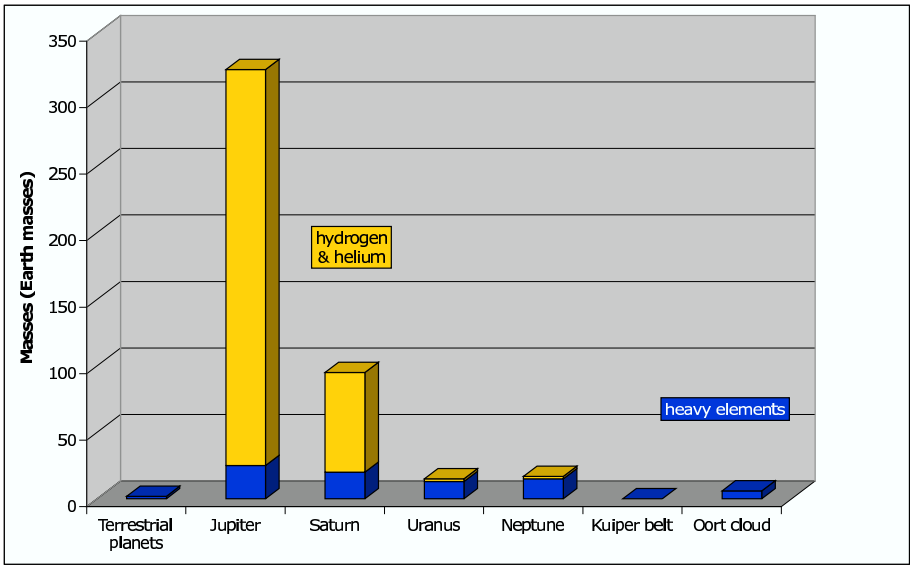

Figure 1. An inventory of hydrogen and helium and all other elements ("heavy elements") in the Solar System excluding the Sun (the Sun has a total mass of 332, 960 $M_\oplus$, including about 5000 $M_\oplus$ in heavy elements, 1 $M_\oplus$ being the mass of the Earth). The precise amount of heavy elements in Jupiter (10 – 40 $M_\oplus$) and Saturn (20 – 30 $M_\oplus$) is uncertain (see § 4.1).

Because of a massive envelope mostly made of hydrogen helium, these planets are *fluid*, with no solid or liquid surface. In terms of structure and composition, they lie in between stars (gaseous and mostly made of hydrogen and helium) and smaller terrestrial planets (solid and liquid and mostly made of heavy elements), with Jupiter and Saturn being closer to the former and Uranus and Neptune to the latter (see fig. 1).

The discovery of many extrasolar planets of masses from a few thousands down to a few Earth masses and the possibility to characterize them by the measurement of their mass and size prompts a more general definition of giant planets. For this review, we will adopt the following: "a giant planet is a planet mostly made of hydrogen and helium and too light to ignite deuterium fusion." This is purposely relatively vague – depending on whether the inventory is performed by mass or by atom or molecule, Uranus and Neptune may be included or left out of the category. Note that Uranus and Neptune are indeed relatively different in structure than Jupiter and Saturn and are generally referred to as "ice giants", due to an interior structure that is consistent with the presence of mostly "ices" (a mixture formed from the condensation in the protoplanetary disk of low- refractivity materials such as H_2O, CH_4 and NH_3, and brought to the high-pressure conditions of planetary interiors – see below).

Globally, this definition encompasses a class of objects that have similar properties (in particular, a low viscosity and a non-negligible compressibility) and inherited part of their material directly from the same reservoir as their parent star. These objects can thus be largely studied with the same tools, and their formation is linked to that of their parent star and the fate of the circumstellar gaseous disk present around the young star.

We will hereafter present some of the key data concerning giant planets in the solar system and outside. We will then present the theoretical basis for the study of their structure and evolution. On this basis, the constraints on their composition will be discussed and analyzed in terms of consequences for planet formation models.

2. Observations and global properties

2.1. Visual appearances

Figure 2. Photomontage from images of Voyager 2 (Jupiter, Uranus, and Neptune) and Cassini (Saturn). The planets are shown to scale, with their respective axial inclinations.

In spite of its smallness, the sample of four giant planets in our solar system exhibits a large variety of appearances, shapes, colors, variability, etc. As shown in Figure 2, all four giant planets are flattened by rotation and exhibit a more or less clear zonal wind pattern, but the color of their visible atmosphere is very different (this is due mostly to minor species in the high planetary atmosphere), their clouds have different compositions (ammonia for Jupiter and Saturn, methane for Uranus and Neptune) and depths, and their global meteorology (number of vortexes, long-lived anticyclones such as Jupiter's Great Red Spot, presence of planetary-scale storms, convective activity) is different from one planet to the next.

We can presently only wonder about what is in store for us with extrasolar giant planets since we cannot image and resolve them. But with orbital distances from as close as 0.01 AU to 100 AU and more, a variety of masses, sizes, and parent stars, we should expect to be surprised!

2.2. Gravity fields

The mass of our giant planets can be obtained with great accuracy from the observation of the motions of their natural satellites: 317.834, 95.161, 14.538 and 17.148 times the mass of the Earth ($1\,M_\oplus = 5.97369 \times 10^{27}$ g) for Jupiter, Saturn, Uranus and Neptune, respectively. More precise measurements of their gravity field can be obtained through the analysis of the trajectories of a spacecraft during flyby, especially when they come close to the planet and preferably in a near-polar orbit. The gravitational field thus measured departs from a purely spherical function due to the planets' rapid rotation. The measurements are generally expressed by expanding the components of the gravity field in Legendre polynomials P_i of progressively higher orders:

$$V_{\rm ext}(r,\theta) = -\frac{GM}{r}\left\{1 - \sum_{i=1}^{\infty}\left(\frac{R_{\rm eq}}{r}\right)^i J_i P_i(\cos\theta)\right\}, \quad (1)$$

where $V_{\rm ext}(r,\theta)$ is the gravity field evaluated outside the planet at a distance r and colatitude θ, $R_{\rm eq}$ is the equatorial radius, and J_i are the gravitational moments. Because the giant planets are very close to hydrostatic equilibrium the coefficients of even order are the only ones that are not negligible. We will see how these gravitational moments, as listed in table 1, help us constrain the planets' interior density profiles.

Table 1 also indicates the radii obtained with the greatest accuracy by radio-occultation experiments. An important consequence obtained is the fact that these planets have low densities, from 0.688 g cm^{-3} for Saturn to 1.64 g cm^{-3} for Neptune, to be compared with densities of 3.9 to 5.5 g cm^{-3} for the terrestrial planets in the solar system. Considering the compression that strongly increases with mass, one is led naturally to the conclusion that these planets contain an important proportion of light materials including hydrogen and helium. It also implies that Uranus and Neptune

Table 1. Characteristics of the gravity fields and radii

	Jupiter	**Saturn**	**Uranus**	**Neptune**
$M \times 10^{-26}$ [kg]	18.986112(15)[a]	5.68463036(16)[b]	0.8683205(34)[c]	1.0243547861(15)[d]
$R_{\rm eq} \times 10^{-7}$ [m]	7.1492(4)[e]	6.0268(4)[f]	2.5559(4)[g]	2.4766(15)[g]
$R_{\rm pol} \times 10^{-7}$ [m]	6.6854(10)[e]	5.4364(10)[f]	2.4973(20)[g]	2.4342(30)[g]
$\overline{R} \times 10^{-7}$ [m]	6.9894(6)[h]	5.8210(6)[i]	2.5364(10)[i]	2.4625(20)[i]
$\overline{\rho} \times 10^{-3}$ [kg m^{-3}]	1.3275(4)	0.6880(2)	1.2704(15)	1.6377(40)
$R_{\rm ref} \times 10^{-7}$ [m]	7.1398[a]	6.0330[b]	2.5559	2.5225[d]
$J_2 \times 10^2$	1.4736(1)[a]	1.629071(27)[b]	0.35160(32)[c]	0.34084(45) [d]
$J_4 \times 10^4$	−5.87(5)[a]	−9.358(28)[b]	−0.354(41)[c]	−0.334(29)[d]
$J_6 \times 10^4$	0.31(20)[a]	0.861(96)[b]	...	...
$P_\omega \times 10^{-4}$ [s]	3.57297(41)[j]	3.83624(47) ?[j,k]	6.206(4)[l]	5.800(20)[m]
q	0.08923(5)	0.15491(10)	0.02951(5)	0.02609(23)
$C/MR_{\rm eq}^2$	0.258	0.220	0.230	0.241

The numbers in parentheses are the uncertainty in the last digits of the given value. The value of the gravitational constant used to calculate the masses of Jupiter and Saturn is $G = 6.67259 \times 10^{-11}$ N m^2 kg^{-2} (Cohen and Taylor, 1987). The values of the radii and density correspond to the one bar pressure level (1 bar= 10^5 Pa). Gravitational moments are normalized at the reference radius $R_{\rm ref}$. Only values published in refereed journals are considered.

[a] Campbell and Synnott (1985)

[b] Jacobson et al. (2006)

[c] Anderson et al. (1987)

[d] Jacobson (2009)

[e] Lindal et al. (1981); Helled and Guillot (2013) derive slightly different values.

[f] Lindal et al. (1985)

[g] Lindal (1992a); Helled et al. (2010) derive slightly different values.

[h] From 4th order figure theory

[i] $(2R_{\rm eq} + R_{\rm pol})/3$ (Clairaut's approximation)

[j] Davies et al. (1986)

[k] This measurement from the *Voyager* era is now in question and values down to 37955 s have been proposed (see § 2.3)

[l] Warwick et al. (1986). See however Helled et al. (2010).

[m] Warwick et al. (1989). See however Helled et al. (2010).

which are less massive must contain a relatively larger proportion of heavy elements than Jupiter and Saturn. This may lead to a sub-classification between the hydrogen-helium giant planets Jupiter and Saturn, and the "ice giants" or "sub giants" Uranus and Neptune.

The planets are also relatively fast rotators, with periods of $\sim$ 10 hours for Jupiter and Saturn, and $\sim$ 17 hours for Uranus and Neptune. The fact that this fast rotation visibly affects the figure (shape) of these planets is seen by the significant difference between the polar and equatorial radii. It also leads to gravitational moments that differ significantly from a null value. However, it is important to stress that there is no unique rotation frame for these fluid planets: atmospheric zonal winds imply that different latitudes rotate at different velocities (see § 2.4), and the magnetic field provides another rotation period. Because the latter is tied to the deeper levels of the planet, it is believed to be more relevant when interpreting the gravitational moments. The rotation periods listed in Table 1 hence correspond to that of the magnetic field. The case of Saturn is complex and to be discussed in the next section.

2.3. Magnetic fields

As the Earth, the Sun and Mercury, our four giant planets possess their own magnetic fields. These magnetic fields $\mathbf{B}$ may be expressed in form of a development in spherical harmonics of the scalar potential W, such that $\mathbf{B} = -\boldsymbol{\nabla} W$:

$$W = a \sum_{n=1}^{\infty} \left(\frac{a}{r}\right)^{n+1} \sum_{m=0}^{n} \left\{ g_n^m \cos(m\phi) + h_n^m \sin(m\phi) \right\} P_n^m(\cos\theta). \quad (2)$$

r is the distance to the planet's center, a its radius, θ the colatitude, ϕ the longitude and P_n^m the associated Legendre polynomials. The coefficients g_n^m and h_n^m are the magnetic moments that characterize the field. They are expressed in magnetic field units.

One can show that the first coefficients of relation (2) (for $n = 0$ and $n = 1$) correspond to the potential of a magnetic dipole such that $W = \mathbf{M} \cdot \mathbf{r}/r^3$ of moment:

$$M = a^3 \left\{ \left(g_1^0\right)^2 + \left(g_1^1\right)^2 + \left(h_1^1\right)^2 \right\}^{1/2}. \tag{3}$$

As shown by the Voyager 2 measurements, Jupiter and Saturn have magnetic fields of essentially dipolar nature, of axis close to the rotation axis (g_1^0 is much larger than the other harmonics); Uranus and Neptune have magnetic fields that are intrinsically much more complex. To provide an idea of the intensity of the magnetic fields, the value of the dipolar moments for the four planets are 4.27 Gauss $\mathrm{R_J^3}$, 0.21 Gauss $\mathrm{R_S^3}$, 0.23 Gauss $\mathrm{R_U^3}$, 0.133 Gauss $\mathrm{R_N^3}$, respectively (Connerney et al., 1982; Acuna et al., 1983; Ness et al., 1986, 1989, see also chapter by Connerney).

A true surprise from *Voyager* that has been confirmed by the *Cassini-Huygens* mission is that Saturn's magnetic field is axisymetric *to the limit of the measurement accuracy*: Saturn's magnetic and rotation axes are perfectly aligned (e.g., Russell and Dougherty, 2010). Voyager measurements indicated nevertheless a clear signature in the radio signal at $10^{\mathrm{h}}39^{\mathrm{m}}22.4^{\mathrm{s}}$ believed to be a consequence of the rotation of the magnetic field. New measurements of a slower spin period of $10^{\mathrm{h}}47^{\mathrm{m}}6^{\mathrm{s}}$ by Cassini (Gurnett et al., 2005; Giampieri et al., 2006) have shown that the kilometric radiation was not directly tied to the period of the magnetic field but resulted from a complex interplay between the spin of the planetary magnetic field and the solar wind (e.g. Cecconi and Zarka, 2005). New periods have been proposed: $10^{\mathrm{h}}32^{\mathrm{m}}35^{\mathrm{s}}$ based on a minimization of the zonal differential rotation (Anderson and Schubert, 2007) and $10^{\mathrm{h}}33^{\mathrm{m}}13^{\mathrm{s}}$ based on the latitudinal distribution of potential vorticity (Read et al., 2009). The problem still stands out.

These magnetic fields must be generated in the conductive parts of the interiors, i.e., in metallic hydrogen at radii which are about 80% and 60% of the planetary radius for Jupiter and Saturn respectively (see sections 3.2, 4.1 and e.g., Stanley and Glatzmaier (2010)). Recent models that consistently join the slowly convecting metallic interior with the non-conducting outer molecular envelope dominated by zonal flows result in a mainly dipolar magnetic field similar to the observations and further show that Jupiter's stronger magnetic field and Saturn's broader equatorial jet (see next section) can be interpreted as resulting from the deeper location of the transition region in Saturn (Heimpel and Gómez Pérez, 2011). These explanations remain largely qualitative rather than quantitative and are further complicated by a necessary overforcing of the simulations (see Showman et al., 2011, and next section). The question of why Saturn's magnetic field is much more axisymmetric than Jupiter's remains. Dipolar fields are obtained relatively naturally through the forcing of zonal jets extending down to the conducting region (Guervilly et al., 2012) but why Jupiter differs is unexplained. A possibility is that both fields are non-axisymmetric at deep levels but that Saturn's is filtered by a more extended helium sedimentation region (Stevenson, 1983), but in practice, a realistic solution yielding Saturn's measured field has not been found (Stanley and Glatzmaier, 2010, and references therein).

Within Uranus and Neptune, the magnetic field is believed to be generated within a layer in which water is in an ionic phase, below about 80% of their total radius (see Redmer et al., 2011, and section 4.2 hereafter). Their complex, multipolar magnetic fields has been thought to be a consequence of a strong stratification and of a dynamo generated in a thin shell (Stanley and Bloxham, 2004). However, this point of view is now challenged by new simulations that generate both planets' magnetic fields and zonal wind structures through a thick shell dynamo (Soderlund et al., 2013). Further work however must involve realistic variations of the interior density and conductivity.

2.4. Atmospheric dynamics: winds and weather

The atmospheres of all giant planets are evidently complex and turbulent in nature. This can, for example, be seen from the mean zonal winds (inferred from cloud tracking), which are very rapidly varying functions of the latitude (see e.g., Ingersoll et al., 1995): while some of the regions rotate at the same speed as the interior magnetic field (in the so-called "system III" reference frame), most of the atmospheres do not. Jupiter and Saturn both have superrotating equators (+100 and +400 m s^{-1} in system III, for Jupiter and Saturn, respectively), Uranus and Neptune have subrotating equators, and superrotating high latitude jets. Neptune, which receives the smallest amount of energy from the Sun has the largest peak-to-peak latitudinal variations in wind velocity: about 600 m s^{-1}. It can be noted that, contrary to the case of the strongly irradiated planets to be discussed later, the winds of Jupiter, Saturn, Uranus and

Neptune, are significantly slower than the planet itself under its own spin (from 12.2 km s^{-1} for Jupiter to 2.6 km s^{-1} for Neptune, at the equator).

It is not yet clear whether the observed winds are driven from the bottom or from the top. The first possibility is that surface winds are related to motions in the planets' interiors, which, according to the Taylor-Proudman theorem, should be confined by the rapid rotation to the plane perpendicular to the axis of rotation (Busse, 1978). This is now backed by simulations in the anelastic limit (i.e., accounting for compressibility) which show that the outcome strongly depends on the density stratification in the interior. A small density contrast (as expected in Jupiter and Saturn) leads to equatorial superrotation whereas for a large one (as expected for Uranus and Neptune), the equatorial jet tends to subrotate (Glatzmaier et al., 2009; Gastine et al., 2013). However, the application of these numerical results to the true conditions prevailing in the giant planets requires an extrapolation over at least 6 orders of magnitude (Showman et al., 2011). The second possibility (not exclusive) is that winds are driven from the top by the injection of turbulence at the cloud level, which can also lead to the correct winds for the four giant planets (Lian and Showman, 2010; Liu and Schneider, 2011).

Information on the gravity field of the planets can be used to constrain the interior rotation profile, as in the case of Uranus and Neptune whose observed jets appear to only extend to the outer 0.15% and 0.20% of the mass (corresponding to pressures of 2 and 4 kbar) for Uranus and Neptune, respectively (Kaspi et al., 2013). The method is promising with the perspective of the Juno measurements at Jupiter (Liu et al., 2013).

Our giant planets also exhibit planetary-scale to small-scale storms with very different temporal variations. For example, Jupiter's great red spot is a 12000 km-diameter anticyclone found to have lasted for at least 300 years (e.g. Simon-Miller et al., 2002). Storms developing over the entire planet have even been observed on Saturn (Sanchez-Lavega et al., 1996). Uranus and Neptune's storm system has been shown to have been significantly altered since the Voyager era (Rages et al., 2002; Hammel et al., 2005; de Pater et al., 2011). On Jupiter, small-scale storms related to cumulus-type cloud systems have been observed (e.g., Gierasch et al., 2000; Hueso et al., 2002), and lightning strikes have been monitored by Galileo (e.g., Little et al., 1999). These represent only a small arbitrary subset of the work concerning the complex atmospheres of these planets.

It is tempting to extrapolate these observations to the objects outside our Solar System as well. However, two features governing the weather in these are not necessarily present for exoplanets (e.g., Guillot, 1999b): their rapid rotation, and the presence of abundant condensing species and in particular one, water, whose latent heat can fuel powerful storms. But as we will see briefly in section 2.10 theoretical models for exoplanets are now complemented by measurements of wind speeds and of global temperature contrasts, offering the perspective of a global approach to planetary weather and atmospheric dynamics.

2.5. Energy balance and atmospheric temperature profiles

Jupiter, Saturn and Neptune are observed to emit more energy than they receive from the Sun (see Table 2). The case of Uranus is less clear. Its intrinsic heat flux $F_{\rm int}$ is significantly smaller than that of the other giant planets. With this caveat, all four giant planets can be said to emit more energy than they receive from the Sun. Hubbard (1968) showed in the case of Jupiter that this can be explained simply by the progressive contraction and cooling of the planets.

Table 2. Energy balance as determined from Voyager IRIS data[a].

	Jupiter	**Saturn**	**Uranus**	**Neptune**
Absorbed power [10^{16} J s^{-1}]	50.14±2.48	11.14±0.50	0.526±0.037	0.204±0.019
Emitted power [10^{16} J s^{-1}]	83.65±0.84	19.77±0.32	0.560±0.011	0.534±0.029
Intrinsic power [10^{16} J s^{-1}]	33.5±2.6	8.63±0.60	$0.034^{+0.038}_{-0.034}$	0.330±0.035
Intrinsic flux [J s^{-1} m^{-2}]	5.44±0.43	2.01±0.14	$0.042^{+0.047}_{-0.042}$	0.433±0.046
Bond albedo []	0.343±0.032	0.342±0.030	0.300±0.049	0.290±0.067
Effective temperature [K]	124.4±0.3	95.0±0.4	59.1±0.3	59.3±0.8
1-bar temperature[b] [K]	165±5	135±5	76±2	72±2

[a] After Pearl and Conrath (1991)

[b] Lindal (1992b)

A crucial consequence of the presence of an intrinsic heat flux is that it requires high internal temperatures ($\sim 10,000$ K or more), and that consequently the giant planets are *fluid* (not solid) (Hubbard (1968); see also Hubbard et al. (1995)). Another consequence is that they are essentially convective, and that their interior temperature profile are close to *adiabats*. We will come back to this in more detail.

The deep atmospheres (more accurately tropospheres) of the four giant planets are indeed observed to be close to adiabats, a result first obtained by spectroscopic models (Trafton, 1967), then verified by radio-occultation experiments by the Voyager spacecrafts, and by the *in situ* measurement from the Galileo probe (fig. 3). The temperature profiles show a temperature minimum, in a region near 0.2 bar called the tropopause. At higher altitudes, in the stratosphere, the temperature gradient is negative (increasing with decreasing pressure). In the regions that we will be mostly concerned with, in the troposphere and in the deeper interior, the temperature always increases with depth. It can be noticed that the slope of the temperature profile in fig. 3 becomes almost constant when the atmosphere becomes convective, at pressures of a fraction of a bar, in the four giant planets.

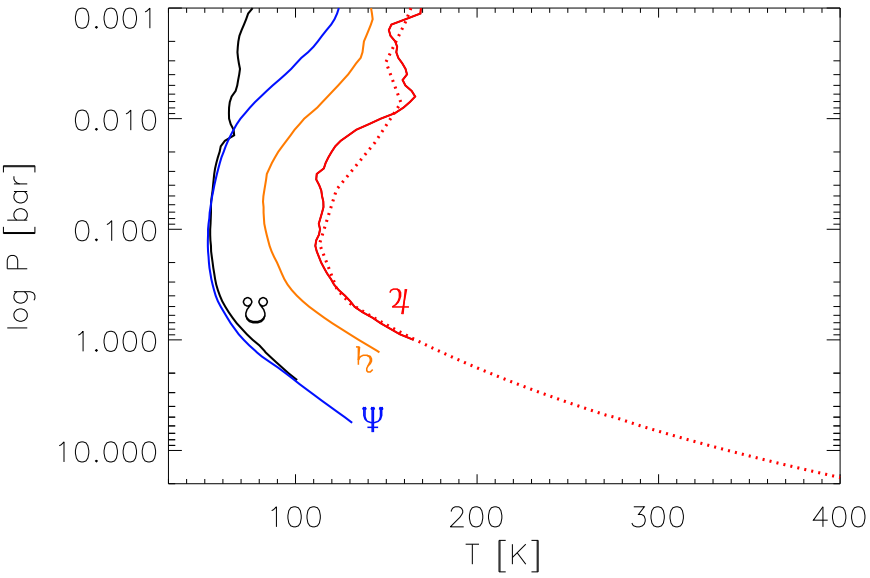

Figure 3. Atmospheric temperatures as a function of pressure for Jupiter, Saturn, Uranus and Neptune, as obtained from Voyager radio-occultation experiments (see Lindal, 1992b). The dotted line corresponds to the temperature profile retrieved by the Galileo probe, down to 22 bar and a temperature of 428 K (Seiff et al., 1998).

It should be noted that the 1 bar temperatures listed in table 2 and the profiles shown in fig. 3 are retrieved from radio-occultation measurements using a helium to hydrogen ratio which, at least in the case of Jupiter and Saturn, was shown to be incorrect. The new values of Y are found to lead to increased temperatures by ~ 5 K in Jupiter and ~ 10 K in Saturn (see Guillot, 1999a). However, the Galileo probe found a 1 bar temperature of 166 K (Seiff et al., 1998), and generally a good agreement with the Voyager radio-occultation profile with the wrong He/H_2 value.

When studied at low spatial resolution, it is found that all four giant planets, in spite of their inhomogeneous appearances, have a rather uniform brightness temperature, with pole-to-equator latitudinal variations limited to a few kelvins (e.g., Ingersoll et al., 1995). However, in the case of Jupiter, some small regions are known to be very different from the average of the planet. This is the case of hot spots, which cover about 1% of the surface of the planet at any given time, but contribute to most of the emitted flux at 5 microns, due to their dryness (absence of water vapor) and their temperature brightness which can, at this wavelength, peak to 260 K.

2.6. Atmospheric compositions

In fluid planets, the distinction between the atmosphere and the interior is not obvious. We name "atmosphere" the part of the planet which can directly exchange radiation with the exterior environment. This is also the part which is accessible by remote sensing. It is important to note that the continuity between the atmosphere and the interior does not guarantee that compositions measured in the atmosphere can be extrapolated to the deep interior, even in a fully convective environment: Processes such as phase separations (e.g., Salpeter, 1973; Stevenson and Salpeter, 1977b; Fortney and Hubbard, 2003), phase transitions (e.g., Hubbard, 1989), chemical reactions (e.g., Fegley and Lodders, 1994) and cloud formation (e.g. Rossow, 1978) can occur and decouple the surface and interior compositions. Furthermore, imperfect mixing may also occur, depending on the initial conditions (e.g., Stevenson, 1985a).

The conventional wisdom is however that these processes are limited to certain species (e.g. helium) or that they have a relatively small impact on the global abundances, so that the hydrogen-helium envelopes may be considered relatively uniform, from the perspective of the global abundance in heavy elements. An important caveat is that measurements must probe deeper than the condensation altitude for any volatile (e.g. ammonia, water, etc.). We first discuss measurements made in the atmosphere before inferring interior compositions from interior and evolution models.

2.6.1. Hydrogen and helium

The most important components of the atmospheres of our giant planets are also among the most difficult to detect: H_2 and He have a zero dipolar moment and hence absorb very inefficiently visible and infrared light. Absorption in the infrared becomes important only at high pressures as a result of collision-induced absorption (e.g., Borysow et al., 1997). On the other hand, lines due to electronic transitions correspond to very high altitudes in the atmosphere, and bear little information on the structure of the deeper levels. The only robust result concerning the abundance of helium in a giant planet is by *in situ* measurement by the Galileo probe in the atmosphere of Jupiter (von Zahn et al., 1998a). The helium mole fraction (i.e., number of helium atoms over the total number of species in a given volume) is $q_{\rm He} = 0.1359 \pm 0.0027$. The helium mass mixing ratio Y (i.e., mass of helium atoms over total mass) is constrained by its ratio over hydrogen, X: $Y/(X + Y) = 0.238 \pm 0.05$. This ratio is by coincidence that found in the Sun's atmosphere, but because of helium sedimentation in the Sun's radiative zone, it was larger in the protosolar nebula: $Y_{\rm proto} = 0.275 \pm 0.01$ and $(X + Y)_{\rm proto} \approx 0.98$ (e.g., Bahcall et al., 1995). Less helium is therefore found in the atmosphere of Jupiter than inferred to be present when the planet formed. We will discuss the consequences of this measurement later: let us mention that the explanation invokes helium settling due to a phase separation in the interiors of massive and cold giant planets.

Helium is also found to be depleted compared to the protosolar value in Saturn's atmosphere. However, in this case the analysis is complicated by the fact that Voyager radio occultations combined with the far-IR sounding (to separate effects of helium from that of temperature) led to a wrong value for Jupiter when compared to the Galileo probe data and hence are suspect for the other planets. The current adopted value from IR data only is now $Y = 0.18 - 0.25$ (Conrath and Gautier, 2000), in agreement with values predicted by interior and evolution models (Guillot, 1999b; Hubbard et al., 1999).

Finally, as shown in table 3 hereafter, Uranus and Neptune are found to have near-protosolar helium mixing ratios, but with considerable uncertainty.

2.6.2. Heavy elements

The abundance of elements other than hydrogen and helium (that we will call hereafter "heavy elements") bears crucial information for the understanding of the processes that led to the formation of these planets. Table 3 summarizes the present situation after *in situ* measurements in Jupiter by the Galileo probe, as well as spectroscopic measurements from spacecraft and from the ground for the other planets.

The elemental abundances in the giant planets' atmospheres are most usefully compared to those in the Sun since they all originated from the protosolar disk. The solar abundances have seen very significant revisions in the past decade because it has been realized that convective motions in the Sun's atmosphere affect spectral lines more extensively than was previously thought. It is not yet clear at this date whether the solar abundances have converged. Furthermore, as discussed for helium, heavy elements gradually settle towards the Sun's interior so that a proper

Table 3. Elemental abundances measured in the tropospheres of giant planets

Element	Carrier	Abundance ratio/H†	Protosun[a]	$\frac{\text{Planet}}{\text{Protosun}}$	Method
Jupiter					
He/H	He	$(7.85 \pm 0.18) \times 10^{-2}$	9.69×10^{-2}	0.810 ± 0.019	Galileo/GPMS [b]
C/H	CH_4	$(1.185 \pm 0.019) \times 10^{-3}$	2.75×10^{-4}	4.31 ± 0.07	Galileo/GPMS[c]
N/H	NH_3	$(3.3 \pm 1.3) \times 10^{-4}$	8.19×10^{-5}	4.05 ± 1.55	Galileo/GPMS[c]
O/H	$H_2O^{\star}$	$(1.49^{+0.98}_{-0.68}) \times 10^{-4}$	6.06×10^{-4}	$0.25^{+0.16}_{-0.11}$	Galileo/GPMS@19 bar[c]
S/H	H_2S	$(4.5 \pm 1.1) \times 10^{-5}$	1.55×10^{-5}	2.88 ± 0.68	Galileo/GPMS[c]
Ne/H	Ne	$(1.20 \pm 0.12) \times 10^{-5}$	1.18×10^{-4}	0.10 ± 0.01	Galileo/GPMS[d]
Ar/H	Ar	$(9.10 \pm 1.80) \times 10^{-6}$	3.58×10^{-6}	2.54 ± 0.50	Galileo/GPMS[d]
Kr/H	Kr	$(4.65 \pm 0.85) \times 10^{-9}$	2.15×10^{-9}	2.16 ± 0.40	Galileo/GPMS[d]
Xe/H	Xe	$(4.45 \pm 0.85) \times 10^{-10}$	2.11×10^{-10}	2.11 ± 0.40	Galileo/GPMS[d]
P/H	$PH_3^{\star}$	$(1.11 \pm 0.06) \times 10^{-6}$	3.20×10^{-7}	3.45 ± 0.18	Cassini/CIRS[e]
Ge/H	$GeH_4^{\star}$	$(4.1 \pm 1.2) \times 10^{-10}$	4.44×10^{-9}	0.09 ± 0.03	Voyager/IRIS[f]
As/H	$AsH_3^{\star}$	$(1.3 \pm 0.6) \times 10^{-10}$	2.36×10^{-10}	0.54 ± 0.27	Ground/IR[g]
Saturn					
He/H	He	$(6.75 \pm 1.25) \times 10^{-2}$	9.69×10^{-2}	0.70 ± 0.13	Voyager/IRIS[h]
C/H	CH_4	$(2.67 \pm 0.11) \times 10^{-3}$	2.75×10^{-4}	9.72 ± 0.41	Cassini/CIRS[i]
N/H	$NH_3^{\star}$	$(2.27 \pm 0.57) \times 10^{-4}$	8.19×10^{-5}	2.77 ± 0.69	Cassini/VIMS[j]
S/H	H_2S	$(1.25 \pm 0.17) \times 10^{-4}$	1.55×10^{-5}	8.08 ± 1.10	Ground/radio[k]
P/H	$PH_3^{\star}$	$(4.65 \pm 0.32) \times 10^{-6}$	3.20×10^{-7}	14.5 ± 1.0	Cassini/CIRS[e]
		$(1.76 \pm 0.17) \times 10^{-6}$	3.20×10^{-7}	5.49 ± 0.53	Cassini/VIMS[i]
		$(4.0^{+1.7}_{-1.1}) \times 10^{-6}$	3.20×10^{-7}	$12.4^{+5.3}_{-3.5}$	Ground/IR[l]
Ge/H	$GeH_4^{\star}$	$(2.3 \pm 2.3) \times 10^{-10}$	4.44×10^{-9}	0.05 ± 0.05	Ground/IR[l]
As/H	$AsH_3^{\star}$	$(1.25 \pm 0.17) \times 10^{-9}$	2.36×10^{-10}	5.33 ± 0.73	Cassini/VIMS[i]
		$(1.71 \pm 0.57) \times 10^{-9}$	2.36×10^{-10}	7.3 ± 2.4	Ground/IR[l]
Uranus					
He/H	He	$(9.0 \pm 2.0) \times 10^{-2}$	9.69×10^{-2}	0.93 ± 0.20	Voyager/IRIS+occult[m]
C/H	$CH_4^{\star}$	$(2.36 \pm 0.30) \times 10^{-2}$	2.75×10^{-4}	85.9 ± 10.7	Hubble/STIS[n]
S/H	$H_2S^{\star}$	$(3.2 \pm 1.6) \times 10^{-4}$	1.55×10^{-5}	21.0 ± 10.5	Ground/radio[o]
Neptune					
He/H	He	$(1.17 \pm 0.20) \times 10^{-1}$	9.69×10^{-2}	1.21 ± 0.20	Voyager/IRIS+occult[p]
C/H	$CH_4^{\star}$	$(1.85 \pm 0.43) \times 10^{-2}$	2.75×10^{-4}	67.5 ± 15.8	Ground/IR[q]
		$(2.47 \pm 0.62) \times 10^{-2}$	2.75×10^{-4}	89.9 ± 22.5	Hubble/STIS[r]
S/H	$H_2S^{\star}$	$(3.2 \pm 1.6) \times 10^{-4}$	1.55×10^{-5}	21.0 ± 10.5	Ground/radio[o]

*: Species which condense or are in chemical disequilibrium, i.e., with vertical/horizontal variations of their concentration. The global elemental abundances are estimated from the maximum measured mixing ratio, but like in the case of H_2O in Jupiter (believed to correspond to the measurement in a dry downdraft), they may only be lower limits to the bulk abundance.

†: Abundance ratios r are measured with respect to atomic hydrogen. In these atmospheres dominated by molecular hydrogen and helium, mole fractions f are found by $f = 2r/(1 + r_{\rm He})$ where $r_{\rm He}$ is the He/H abundance ratio.

[a]: protosolar abundances from Lodders et al. (2009); [b]: von Zahn et al. (1998b); [c]: Wong et al. (2004); [d]: Atreya et al. (2003); [e]: Fletcher et al. (2009a); [f]: Kunde et al. (1982); [g]: Noll et al. (1990); [h]: Conrath and Gautier (2000); [i]: Fletcher et al. (2009b); [j]: Fletcher et al. (2011); [k]: Briggs and Sackett (1989); [l]: Noll and Larson (1991); [m]: Conrath et al. (1987); [n]: Sromovsky et al. (2011); [o]: de Pater et al. (1991); [p]: Conrath et al. (1991); [q]: Baines and Smith (1990); [r]: Karkoschka and Tomasko (2011).

reference for the giant planets is not the solar atmosphere today, but its value 4.5 billion years ago which is model-dependent. Table 3 provides the values obtained for the protosun by Lodders et al. (2009). These are used as reference without accounting for their uncertainties.

The most abundant heavy elements in the envelopes of our four giant planets are O (presumably) and C, N and S. It is possible to model the chemistry of gases in the tropospheres from the top of the convective zone down to the 2000 K temperature level (Fegley and Lodders, 1994). Models conclude that, whatever the initial composition in these elements of planetesimals which collapsed with hydrogen onto Jupiter and Saturn cores during the last phase of the planetary formation, C in the upper tropospheres of giant planets is mainly in the form of gaseous CH_4, N in the form of NH_3, S in the form of H_2S, and O in the form of H_2O. All these gases but methane in Jupiter and Saturn condense in the upper troposphere and vaporize at deeper levels when the temperature increases. Noble gases do not condense even at the tropopauses of Uranus and Neptune, the coldest regions in these atmospheres.

Jupiter is the planet which has been best characterized thanks to the measurements of the Galileo atmospheric probe which precisely measured the abundances of He, Ne, Ar, Kr, Xe, CH_4, NH_3, H_2S, and H_2O down to pressures around 22 bars. As helium, neon was found to be depleted compared to the protosolar value, in line with theoretical predictions that this atom would fall in with the helium droplets (Roulston and Stevenson, 1995; Wilson and Militzer, 2010, and section 3.2.2). C, N, and S were found to be supersolar by a factor 2.5 to 4.5 (Wong et al., 2004), which was not unexpected because condensation of nebula gases results in enriching icy grains and planetesimals. The surprise came from Ar, Kr, Xe, which were expected to be solar because they are difficult to condense, but turned out to be supersolar by a factor ~ 2 (Owen et al., 1999; Wong et al., 2004).

H_2O is difficult to measure in all four giant planets because of its condensation relatively deep. It was hoped that the Galileo probe would provide a measurement of its deep abundance, but the probe fell into one of Jupiter's 5-micron hot spots, now believed to be a dry region mostly governed by downwelling motions (e.g., Showman and Ingersoll, 1998). As a result, and although the probe provided measurements down to 22 bars, well below water's canonical 5 bar cloud base, it is believed that this measurement of a water abundance equal to a fraction of the solar value is only a lower limit. An indirect determination comes from the measurement of the disequilibrium species CO which has to be transported fast from the deep levels where H_2O and CH_4 tend to form more CO (and H_2). This predicts a mostly solar to slightly supersolar (by a factor 2) abundance of O in Jupiter (Visscher and Moses, 2011) and much larger enrichments in Neptune (Lodders and Fegley, 1994). This however depends crucially on the reaction network and somewhat on assumptions on mixing, both of which are not well known. The abundance of oxygen, the most abundant element in the Universe after hydrogen and helium and a crucial planetary building block is essentially unknown for what concerns our four giant planets.

Three other species can help us probe the bulk elemental abundance inside Jupiter, although with larger difficulties perhaps because they are not necessarily in chemical equilibrium at the levels where they are detected and their measured abundances are thus not necessarily representative of their bulk abundance: these are PH_3, GeH_4 and AsH_3. All three where detected remotely rather than in situ. The first one is clearly supersolar in Jupiter, with an enrichment in between that measured for C and S. GeH_4 is clearly subsolar, but this is not surprising because of condensation into solid Ge and GeS (Fegley and Lodders, 1994). The same chemical models would predict that the measured abundance of AsH_3 should be close to its bulk abundance. The measured abundance therefore could be interpreted as a subsolar bulk abundance of As, but with considerable uncertainty.

Table 3 shows that Saturn's atmosphere is more enriched in heavy elements than Jupiter. Unfortunately, unlike Jupiter, no in situ measurement has been performed in this planet and we can only rely on remote sensing. But we can confidently assess that the abundances of C, S, P and As are significantly higher than in Jupiter. Saturn has about twice more C (as CH_4) and S (as H_2S) than Jupiter, for a given mass of atmosphere. The situation for PH_3 is unclear, both because it is highly variable both vertically and latitudinally: the enrichment could be only slightly more than in Jupiter to more than 4 times that value (Fletcher et al., 2009a, 2011). Note that in the presence of horizontal variability (as for this molecule) table 3 indicates the maximum abundances measured - which should be closer to the bulk abundance, except if there exist mechanisms to preferentially trap certain species. The enrichment in N (as NH_3) is smaller than in Jupiter. This may be due to its condensation deeper as NH_4SH (Gulkis et al., 1978), although it does not explain why Jupiter and Saturn would be that different in that respect. The enrichment in As (as AsH_4) is considerably larger than in Jupiter, which is also a mystery (Fletcher et al., 2009b). At least, GeH_4 appears to be of equally low abundance in both planets, but this is probably more related to its condensation than to its bulk abundance.

Finally, Uranus and Neptune provide all signs of a significant enrichment in heavy elements, even though very few

elements have been detected. Methane is the most important one, although the fact that it condenses in these planets complicates the interpretation of the spectroscopic measurements. Large-scale variations with latitude are observed, in particular in Uranus (Sromovsky et al., 2011), but less so in Neptune (Karkoschka and Tomasko, 2011). However, the deep abundances provided in table 3 are very similar for both planets, with a $\sim$ 90 times solar enrichment. This is much higher than the $\sim$ 30 times solar enrichments discussed in past reviews (e.g., Gautier et al., 1995) for two reasons: one is a decrease of the protosolar abundance itself. The other is the fact that it relied on spectroscopic measurements probing higher atmospheric levels affected by methane condensation (see Karkoschka and Tomasko, 2011).

The other key species detected in Uranus and Neptune thanks to ground-based radio observations is H_2S, which points to a 10 to 30 enrichment in sulfur (de Pater et al., 1991). Because this element condenses at even greater depths than methane, the bulk abundance of S in these planets may be larger if the global circulation is indeed important down to the deep levels probed by the radio waves. The measurement is however a difficult one, with other potential absorbers affecting the smooth microwave spectra yielding degenerate solutions.

Overall, the global picture that can be drawn is that of an increase of the abundance of heavy elements compared to the solar value with increasing distance to the Sun, from Jupiter which shows a $\sim$ 2 to 4 enrichment, Saturn a 3 to 10 one, and Uranus and Neptune which are enriched by a factor $\sim$ 90 in carbon and by at least 10 to 30 in sulfur. In spite of their different atmospheric dynamics, and with the present accuracy of the measurements, the two ice giants have very similar abundances.

2.7. Isotopic ratios

Table 4. Isotopic ratios measured in the tropospheres of giant planets

Isotope	Isotopic ratio	Protosun[a]	Planet/Protosun	Comments
Jupiter				
D/H	$(2.25 \pm 0.35) \times 10^{-5}$	1.94×10^{-5}	1.16 ± 0.18	ISO/SWS[q]
$^{3}He/^{4}He$	$(1.66 \pm 0.06) \times 10^{-4}$	1.66×10^{-4}	1.00 ± 0.03	Galileo/GPMS[d]
$^{13}C/^{12}C$	$(1.08 \pm 0.05) \times 10^{-2}$	1.12×10^{-2}	1.04 ± 0.05	Galileo/GPMS[d]
$^{15}N/^{14}N$	$(2.30 \pm 0.30) \times 10^{-3}$	2.27×10^{-3}	0.99 ± 0.13	Galileo/GPMS[d]
$^{22}Ne/^{20}Ne$	$(7.7 \pm 1.2) \times 10^{-2}$	7.35×10^{-2}	0.96 ± 0.15	Galileo/GPMS[d]
$^{38}Ar/^{36}Ar$	$(1.79 \pm 0.08) \times 10^{-1}$	1.82×10^{-1}	1.02 ± 0.05	Galileo/GPMS[d]
$^{128}Xe/Xe$	$(1.80 \pm 0.20) \times 10^{-2}$	2.23×10^{-2}	1.24 ± 0.14	Galileo/GPMS[d]
$^{129}Xe/Xe$	$(2.85 \pm 0.21) \times 10^{-1}$	2.75×10^{-1}	0.96 ± 0.07	Galileo/GPMS[d]
$^{130}Xe/Xe$	$(3.80 \pm 0.50) \times 10^{-2}$	4.38×10^{-2}	1.15 ± 0.15	Galileo/GPMS[d]
$^{131}Xe/Xe$	$(2.03 \pm 0.18) \times 10^{-1}$	2.18×10^{-1}	1.07 ± 0.10	Galileo/GPMS[d]
$^{132}Xe/Xe$	$(2.90 \pm 0.20) \times 10^{-1}$	2.64×10^{-1}	0.91 ± 0.06	Galileo/GPMS[d]
$^{134}Xe/Xe$	$(9.10 \pm 0.70) \times 10^{-2}$	9.66×10^{-2}	1.06 ± 0.08	Galileo/GPMS[d]
Saturn				
D/H	$(1.60 \pm 0.20) \times 10^{-5}$	1.94×10^{-5}	0.83 ± 0.11	Cassini/CIRS[h]
	$(1.70^{+0.75}_{-0.45}) \times 10^{-5}$	1.94×10^{-5}	$0.88^{+0.39}_{-0.23}$	ISO/SWS[q]
$^{13}C/^{12}C$	$(1.09 \pm 0.10) \times 10^{-2}$	1.12×10^{-2}	1.03 ± 0.09	Cassini/CIRS[h]
Uranus				
D/H	$(4.40 \pm 0.40) \times 10^{-5}$	1.94×10^{-5}	2.27 ± 0.21	Herschel/PACS[r]
Neptune				
D/H	$(4.10 \pm 0.40) \times 10^{-5}$	1.94×10^{-5}	2.11 ± 0.21	Herschel/PACS[r]

[a]: protosolar abundances from Lodders et al. (2009), except $^{15}N/^{14}N$ which is corrected by Marty et al. (2011); [d]: Atreya et al. (2003); [h]: Fletcher et al. (2009b); [q]: Lellouch et al. (2001); [r]: Feuchtgruber et al. (2013).

The measurement of isotopic ratios in planetary atmospheres is a powerful tool to understand their origin. Table 4 provides the ensemble of isotopic ratios measured in our giant planets, and a comparison to their values in the Sun.

Of course, the Galileo probe and its onboard mass spectrometer have provided us a strikingly clear picture of Jupiter's atmosphere: it is directly formed from the same material as our Sun, with isotopic ratios which are, to the

accuracy of the measurements, indistinguishable (i.e., within 2 sigma) from the solar values and for elements as diverse as D, He, C, N, Ne, Ar and Xe with as many as 6 isotopes measured. This was expected because indeed Jupiter's composition is globally similar to that of the Sun, but given the fact that the abundances of elements are far from being Sun-like, it is perhaps surprising to find such a good match! By extension, this applies to Saturn although only the deuterium to hydrogen and $^{13}C/^{12}C$ isotopic ratios could be measured by remote spectroscopic observations. This confirms that the atmospheres and envelopes of Jupiter and Saturn originated from the same material that formed the Sun and that mechanisms leading to isotopic fractionation (e.g., atmospheric evaporation) were of limited importance.

In the case of Uranus and Neptune, only the deuterium to hydrogen ratio was measured, from the ground in the infrared (Irwin et al., 2014) and most precisely by recent far infrared spectroscopy from Herschel (Feuchtgruber et al., 2013). Interestingly, it is about twice larger than the protosolar value, and a factor 2 to 6 times smaller than the D/H value in comets. Given our present knowledge of the interiors of Uranus and Neptune, Feuchtgruber et al. (2013) conclude that either these planets contain much more rocks than expected or that the ices in their interior have not been fully mixed.

2.8. Moons and rings

A discussion of our giant planets motivated by the opportunity to extrapolate the results to objects outside our solar system would be incomplete without mentioning the moons and rings that these planets all possess (see chapters by Breuer & Moore, by Peale & Canup and by Hussmann et al.). First, the satellites/moons can be distinguished from their orbital characteristics as regular or irregular. The first ones have generally circular, prograde orbits. The latter tend to have eccentric, extended, and/or retrograde orbits.

These satellites are numerous: After the Voyager era, Jupiter was known to possess 16 satellites, Saturn to have 18, Uranus 20 and Neptune 8. Recent extensive observation programs have seen the number of satellites increase considerably, with a growing list of satellites presently reaching 62, 56, 27 and 13 for Jupiter, Saturn, Uranus and Neptune, respectively. All of the new satellites discovered since Voyager are classified as irregular.

The presence of regular and irregular satellites is due in part to the history of planet formation. It is believed that the regular satellites have mostly been formed in the protoplanetary subnebulae that surrounded the giant planets (at least Jupiter and Saturn) at the time when they accreted their envelopes. On the other hand, the irregular satellites are thought to have been captured by the planet. This is, for example, believed to be the case of Neptune's largest moon, Triton, which has a retrograde orbit.

A few satellites stand out by having relatively large masses: it is the case of Jupiter's Io, Europa, Ganymede and Callisto, of Saturn's Titan, and of Neptune's Triton. Ganymede is the most massive of them, being about twice the mass of our Moon. However, compared to the mass of the central planet, these moons and satellites have very small weights: 10^{-4} and less for Jupiter, $1/4000$ for Saturn, $1/25000$ for Uranus and $1/4500$ for Neptune. All these satellites orbit relatively closely to their planets. The farthest one, Callisto revolves around Jupiter in about 16 Earth days.

The four giant planets also have rings, whose material is probably constantly resupplied from their satellites. The ring of Saturn stands out as the only one directly visible with binoculars. In this particular case, its enormous area allows it to reflect a sizable fraction of the stellar flux arriving at Saturn, and makes this particular ring as bright as the planet itself. The occurrence of such rings would make the detection of extrasolar planets slightly easier, but it is yet unclear how frequent they can be, and how close to the stars rings can survive both the increased radiation and tidal forces.

2.9. Seismology

The best way to directly probe planetary (or stellar) interiors is through seismology, i.e., by measuring the spectrum of waves propagating through the interior. Our knowledge of the interior structure of the Earth, the Sun and even other stars is largely due to the ability to detect the oscillations of these objects. Because Jupiter (and by extent the other giant planets in our Solar System) are similar in composition and density to the Sun, the possibility to detect pressure waves in their atmosphere has been proposed in the 1970's. In particular, Vorontsov et al. (1976) showed that waves with periods smaller than about 10 minutes would be trapped and reflected downwards in Jupiter's and Saturn's atmospheres, creating the possibility for resonant waves similar to those observed in the Sun to exist. On the theoretical side, the possibility of how these waves may be excited has however remained problematic (e.g., Bercovici and Schubert, 1987).

After two decades of promising but slow progress, the case for the existence of detectable free oscillations of giant planets has recently taken a new turn. First, using ground-based Doppler imaging of Jupiter, Gaulme et al. (2011) detected an oscillation pattern with frequencies between 0.8 and 2 mHz and a characteristic spacing of the peak of $155.3 \pm 2.2\,\mu$Hz, in agreement with theoretical models. Separately, Hedman and Nicholson (2013) confirmed that waves observed by the Cassini spacecraft in Saturn's rings cannot be caused by satellites and therefore must result from oscillations in Saturn, as had been proposed by Marley and Porco (1993).

Further observations are required to better characterize the oscillations of these planets and start using them as probes of the planetary interiors (e.g., Jackiewicz et al., 2012). This is very promising however and should lead to a revolution in our understanding of the giant planets.

2.10. Exoplanets

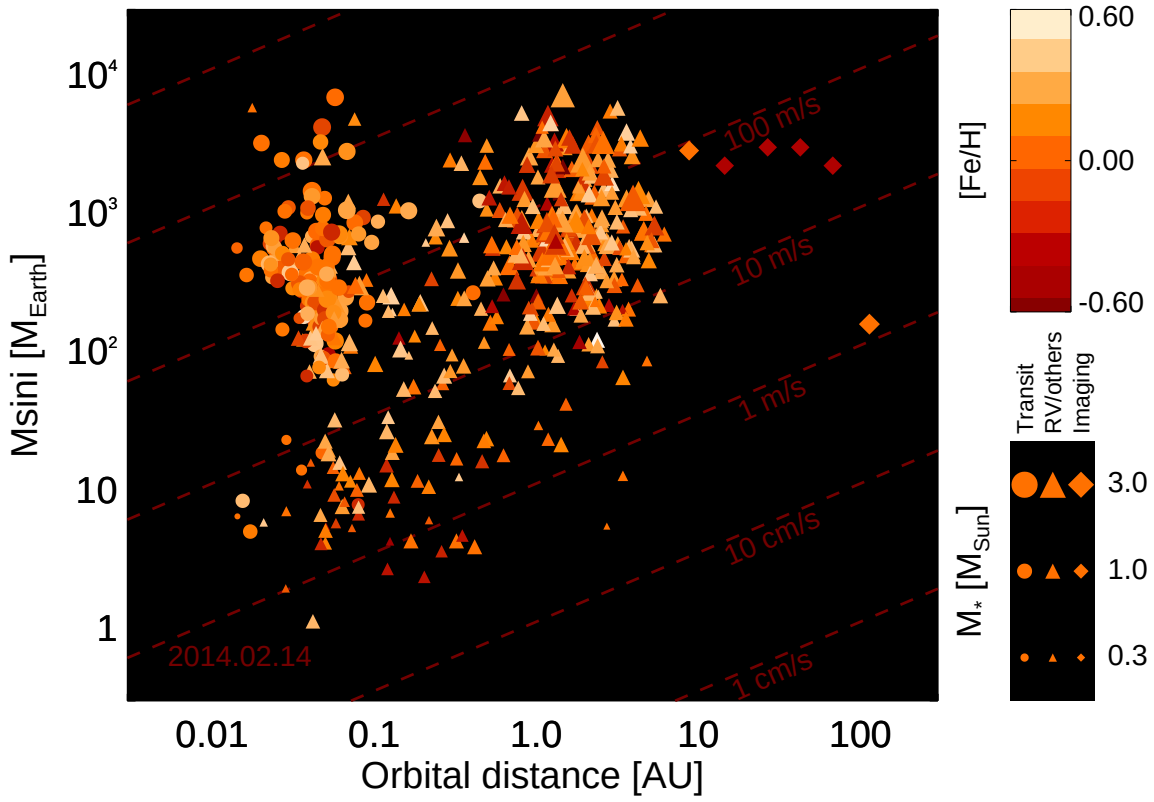

Figure 4. Masses and orbital distances of the extrasolar planets discovered by early 2014. Planets detected in transit are shown with circles, those detected by direct imaging with diamonds. All other systems (mostly detected by radial velocimetry) are shown as triangles. In the case of planets discovered by radial velocimetry, the displayed masses correspond to masses multiplied by the sine of the unknown inclination. The size of the symbols is proportional to the mass of the parent star (from 0.1 to 3.1 stellar masses). The color (from reddish to white) is proportional to the stellar metallicity (from [Fe/H] = −0.8 to 0.6). The radial velocimetry thresholds from 1 cm/s to 10 km/s are indicated as dashed lines.

Huge progress has been made in the field of extrasolar planets since the detection of the first giant planet orbiting a solar-type star by Mayor and Queloz (1995). As shown in figure 4, more than a thousand planets are known at the time of this review, and importantly, more than four hundred planets that transit their star at each orbital revolution have been identified (Wright et al., 2011; Schneider et al., 2011). These transiting planets are especially interesting because of the possibility to measure both their mass and size and thus obtain constraints on their global composition.

In spite of their particular location just a few stellar radii away from their stars, the transiting giant planets that have been discovered bear some resemblance with their Solar System cousins in the sense that they are also mostly

made of hydrogen and helium (e.g., Burrows et al., 2000; Guillot, 2005; Baraffe et al., 2005). They are, however, much hotter due to the intense irradiation that they receive.

Although obtaining direct information on these planets represents a great observational challenge, several key steps have been accomplished: Atomic sodium, predicted to be detectable (Seager and Sasselov, 2000), has indeed been detected by transit spectroscopy(Charbonneau et al., 2002) early on, and a tentative abundance measured in planet HD209458 b: According to Sing et al. (2009), it appears to be oversolar by a factor ~ 2 at pressures deeper than about ~ 3 mbar and undersolar above that level (see also Vidal-Madjar et al., 2011). Hydrodynamically escaping species (including hydrogen, oxygen, carbon, nitrogen and heavier ions) have also been detected around the brightest hot Jupiters (e.g., Vidal-Madjar et al., 2003; Fossati et al., 2010; Bourrier et al., 2013). A theoretical study of the atmospheric dynamics of hot Jupiters (Showman and Guillot, 2002) predicted strong day-night temperature variations (up to 100's K), fast km/s zonal jets and a displacement of the hottest point west of the substellar point. These have been confirmed by observations of transiting and non-transiting planets in the infrared (Harrington et al., 2006; Knutson et al., 2007) and by doppler-imaging of planetary CO lines (Snellen et al., 2010).

Unfortunately, the list of chemical species thought to have been detected (see Seager and Deming, 2010, for a review) has dwindled in recent years due to the realization that instrumental effects could mimic spectral signatures (e.g., Désert et al., 2009; Gibson et al., 2011; Crouzet et al., 2012), due to new observations with a better instrument (e.g., Deming et al., 2013) and generally because of the unexpected prevalence of hazes in these close-in exoplanets (e.g., Sing et al., 2009; Pont et al., 2013). After examination, claims of a high C/O ratio in some of these atmospheres also appear to be highly uncertain (Crossfield et al., 2012).

In any case, in spite of the hiccups, there is obviously a big potential for growth in this young field, and the comparison between fine observations made for giant planets in our Solar System and the more crude, but also more statistically significant data obtained for planets around other stars promise to be extremely fruitful to better understand these objects.

3. The calculation of interior and evolution models

3.1. Basic equations

The structure and evolution of a giant planet is governed by the following hydrostatic, thermodynamic, mass conservation and energy conservation equations:

$$\frac{\partial P}{\partial r} = -\rho g \tag{4}$$

$$\frac{\partial T}{\partial r} = \frac{\partial P}{\partial r}\frac{T}{P}\nabla_T. \tag{5}$$

$$\frac{\partial m}{\partial r} = 4\pi r^2 \rho. \tag{6}$$

$$\frac{\partial L}{\partial r} = 4\pi r^2 \rho\left(\dot{\epsilon} - T\frac{\partial S}{\partial t}\right), \tag{7}$$

where P is the pressure, ρ the density, and $g = Gm/r^2$ the gravity (m is the mass, r the radius and G the gravitational constant). The temperature gradient $\nabla_T \equiv (d\ln T/d\ln P)$ depends on the process by which the internal heat is transported. L is the intrinsic luminosity, t the time, S the specific entropy (per unit mass), and $\dot{\epsilon}$ accounts for the sources of energy due e.g., to radioactivity or more importantly nuclear reactions. Generally it is a good approximation to assume $\dot{\epsilon} \sim 0$ for objects less massive than $\sim 13\,M_J$, i.e., too cold to even burn deuterium (but we will see that in certain conditions this term may be useful, even for low mass planets).

The boundary condition at the center is trivial: $r = 0$; ($m = 0$, $L = 0$). The external boundary condition is more difficult to obtain because it depends on how energy is transported in the atmosphere. One possibility is to use the Eddington approximation, and to write (e.g., Chandrasekhar, 1939): $r = R$; ($T_0 = T_{\rm eff}$, $P_0 = 2/3\, g/\kappa$), where $T_{\rm eff}$ is the effective temperature (defined by $L = 4\pi R\sigma T_{\rm eff}^4$, with σ being the Stephan-Boltzmann constant), and κ is a mean opacity. Note for example that in the case of Jupiter $T_{\rm eff} = 124\,$K, $g = 26\,{\rm m\,s^{-2}}$ and $\kappa \approx 5\times10^{-3}(P/1\,{\rm bar})\,{\rm m^2\,kg^{-1}}$. This implies $P_0 \approx 0.2\,$bar (20,000 Pa), which, given the simplicity of the calculation, is surprisingly close to the

location of Jupiter's real tropopause where $T \approx 110$ K. Actually, the properties of the opacities of important absorbing chemical species like water and their pressure dependence imply that photospheres around 0.1 bar should be common (Robinson and Catling, 2014).

However, the Eddington boundary condition should not be used in the case of irradiated atmospheres because it does not properly account for both the incoming flux (mostly at visible wavelengths for planets around solar-type stars) and the intrinsic flux (in the infrared). The fact that opacities differ at these wavelengths yields the possibility of thermal inversions (higher visible than infrared opacities) or a greenhouse effect (lower visible than infrared opacities) and thus a hotter interior, something that cannot be captured without accounting for the different fluxes. Analytical solutions of the radiative transfer problem exist in the semi-grey case (two opacities for the visible and infrared, respectively) (Hansen, 2008; Guillot, 2010), and can even be extended to include non-grey effects (Parmentier and Guillot, 2014). Numerical solutions in the non-irradiated, solar-composition case are provided by Saumon et al. (1996), and for the irradiation levels and compositions relevant for the solar system giant planets by Fortney et al. (2011). In that case, a grid is used to relate the atmospheric temperature and pressure at a given level to the radius R, intrinsic luminosity L and incoming stellar luminosity $L_{*\rm p}$: $r = R$; ($T_0 = T_0(R, L, L_{*\rm p})$, $P_0 = P_0(R, L, L_{*\rm p})$). P_0 is chosen to satisfy the condition that the corresponding optical depth at that level should be much larger than unity.

3.2. High pressure physics & equations of state

3.2.1. Hydrogen

In terms of pressures and temperatures, the interiors of giant planets lie in a region for which accurate equations of state (EOS) are extremely difficult to calculate. This is because both molecules, atoms, and ions can all coexist, in a fluid that is partially degenerate (free electrons have energies that are determined both by quantum and thermal effects) and partially coupled (Coulomb interactions between ions are not dominant but must be taken into account). The presence of many elements and their possible interactions further complicate matters. For lack of space, this section will mostly focus on hydrogen whose EOS has seen the most important developments in recent years. A phase diagram of hydrogen (fig. 5) illustrates some of the important phenomena that occur in giant planets.

The photospheres of giant planets are generally relatively cold (50 to 3000 K) and at low pressure (0.1 to 10 bar, or 10^4 to 10^6 Pa), so that hydrogen is in molecular form and the perfect gas conditions apply. As one goes deeper into the interior hydrogen and helium progressively become fluid. (The perfect gas relation tends to underestimate the pressure by 10% or more when the density becomes larger than about 0.02 g cm^{-3} ($P \gtrsim 1$ kbar in the case of Jupiter)).

Characteristic interior pressures are considerably larger however: as implied by Eqs. 4 and 6, $P_{\rm c} \approx GM^2/R^4$, of the order of 10-100 Mbar for Jupiter and Saturn. As shown in fig. 5, all the central pressures and temperatures of giant planets and brown dwarfs (from Uranus to CoRoT-15b) lie in a regime of high pressures and temperatures lower than the corresponding Fermi temperature $T_{\rm F}$, implying that electrons are degenerate: their pressure is mostly a function of the density of the material. In Jupiter and Saturn, the degeneracy parameter $\theta = T/T_{\rm F}$ is always close to 0.03. Even for the warmer CoRoT-15b (a $\sim 60\,{\rm M_{Jup}}$ brown dwarf discovered in transit in front of its parent star – see Bouchy et al. (2011)), $\theta \approx 0.2$. This implies that for these objects, the thermal component is small so that the energy of electrons in the interior is expected to be only slightly larger than their non-relativistic, fully degenerate limit: $u_{\rm e} \geq 3/5\, kT_{\rm F} = 15.6\,(\rho/\mu_{\rm e})^{2/3}$ eV, where k is Boltzmann's constant, $\mu_{\rm e}$ is the number of nucleons per electron and ρ is the density in g cm^{-3}. For pure hydrogen, when the density reaches ~ 0.8 g cm^{-3}, the average energy of electrons becomes larger than hydrogen's ionization potential, even at zero temperature: hydrogen pressure-ionizes and becomes metallic. This molecular to metallic transition occurs near Mbar pressures, but exactly how this happens is a result of the complex interplay of thermal, Coulomb and degeneracy effects.

Recent laboratory measurements on fluid deuterium have been able to reach extremely high pressures up to 20 Mbar (Mochalov et al., 2012). Beyond that experimental feat, most of the progress of the decade in the domain has been the improvement in our understanding of the hydrogen metallization region at pressures of a fraction to a few Mbars, both from an experimental and numerical point of view (see the very complete review by McMahon et al., 2012). Already in the 1990's, gas-gun experiments had been able to measure a rise in the conductivity of molecular hydrogen up to $T \sim 3000$ K, $P \sim 1.4$ Mbar, a sign that metallization had been reached (Weir et al., 1996). A very sharp transition, probably discontinuous, was then later measured by isentropic convergent explosive shock experiments (Fortov et al., 2007) at pressures between 1.5 and 2.5 Mbar but uncertain temperatures below 4000 K(see McMahon et al., 2012). New experiments at higher temperatures using laser compression, directly (Sano et al., 2011) and from

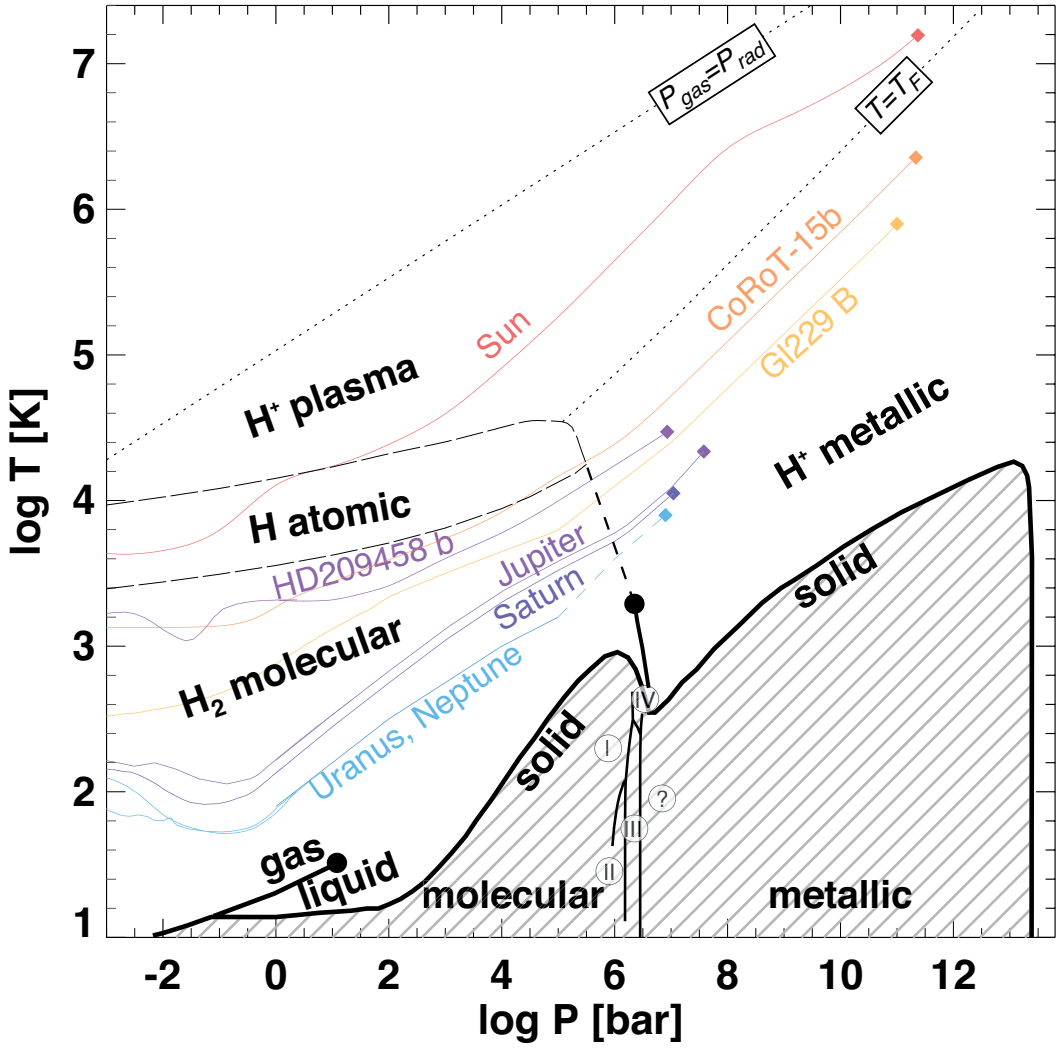

Figure 5. Phase diagram for hydrogen in the pressure-temperature plane, with pressure in bars (1 bar = 10^5 Pa = 10^6 dyn cm^{-2}). The thick lines indicate the first order (discontinuous) phase transitions, the black circles the critical points (McMahon et al., 2012; Morales et al., 2013b). Phase transitions in solid hydrogen with the different known phases are labelled I, II, III, IV (McMahon et al., 2012). The region where 50% of all hydrogen is in atomic form (from Saumon et al., 1995) is shown by a thin contour. The approximate location of the molecular to metallic hydrogen (continuous) transition (Loubeyre et al., 2012; Morales et al., 2013b) is indicated by a dashed line. The $T = T_F$ line separate the non-degenerate region (at low pressures and high temperatures) from the region in which electrons are degenerate (see text). The $P_{gas} = P_{rad}$ line shows the region which is dominated by radiation pressure (at high temperatures). Colored lines show profiles for a selection of noteworthy substellar objects: giant planets from Uranus to Jupiter (Guillot, 2005), the hot Jupiter HD 209458 b (Guillot and Showman, 2002; Burrows, 2013), the brown dwarfs Gl 229 B (Marley et al., 1996), CoRoT-15 b (Bouchy et al., 2011) and our Sun (Christensen-Dalsgaard et al., 1996). The diamonds correspond to the conditions either at the core/envelope interface for Jupiter and Saturn or at the center for the other objects.

precompressed targets (Loubeyre et al., 2012), confirmed that this transition from a weakly conducting molecular fluid to a metal-like hydrogen fluid occurs around pressures near 1 Mbar and temperatures as high as 15,000 K, but that it is continuous at these temperatures. In parallel, *ab initio* calculations of the behavior of fluid hydrogen in this thermodynamical regime predicted the existence of a first order liquid-liquid phase transition (the so-called PPT for *Plasma Phase Transition*) with a critical point near $T \sim 1500 - 2000$ K and $P \sim 2.2$ Mbar (Morales et al., 2010, 2013b). This discontinuous transition at low temperatures merges into a continuous transition at temperatures above the critical point, in good agreement with the experimental data. The PPT is indicated by a thick almost vertical line in fig. 5. It is prolonged by a dashed line indicating the location of the continuous transition from molecular to metallic hydrogen that extends up to the region of thermal dissociation and ionization of hydrogen.

The controversy that had arisen between laser-induced shock compression (da Silva et al., 1997; Collins et al., 1998) and pulsed-power shock compression (Knudson et al., 2004) regarding the maximum compression of deuterium along the principal shock Hugoniot has now been resolved in favor of the latter thanks to new experiments (Boriskov et al., 2005; Hicks et al., 2009) and the realization that the equation of state of quartz used to calibrate the laser-induced shock experiments was incorrect (Knudson and Desjarlais, 2009). Similarly, the existence of a PPT of hydrogen at high temperatures in a regime crossing the adiabats of Jupiter and Saturn (Saumon et al., 1995) have now been shown to be a spurious effect resulting from the different treatment of molecules, atom and ions within the so-called chemical picture (Chabrier et al., 2007). Both laboratory experiments and independent models based on first-principles (Militzer et al., 2001; Desjarlais, 2003; Bonev et al., 2004; Vorberger et al., 2007; French et al., 2012) now agree and show that the transition from molecular to metallic hydrogen should occur continuously in all known giant planets.

Progress has also been made on the issue of the solidification of hydrogen (see McMahon et al., 2012, and references therein). This has led to the confirmation that the interiors of the hydrogen-helium giant planets and brown dwarfs are *fluid* whatever their age, a result expected since the pioneering study by Hubbard (1968). Of course, because of their initial gravitational energy, these objects are warm enough to avoid the critical point for the liquid gas transition in hydrogen and helium, at very low temperatures, but they also lie comfortably above the solidification lines for hydrogen and helium. (An *isolated* Jupiter should begin partial solidification only after at least $\sim 10^3$ Ga of evolution.) They are considered to be fluid because at the high pressures and relatively modest temperatures in their interiors, Coulomb interactions between ions play an important role in the EOS and yield a behavior that is more reminiscent of that of a liquid than that of a gas, contrary to what is the case in e.g., solar-like stars. For Uranus and Neptune, the situation is actually more complex because at large pressures they are not expected to contain a significant amount of hydrogen (see next section).

As fig. 5 highlights, while some highly irradiated planets and brown dwarfs like CoRoT-15b have temperature profiles that get close to the hydrogen thermal dissociation line, most of them are well within the molecular hydrogen regime at low-pressures and in the metallic, degenerate regime at high pressures. Stars like our Sun lie in a higher temperature regime for which the EOS is dominated by thermal effects and electrons are essentially non-degenerate.

3.2.2. Other elements and mixtures

Hydrogen is of course a key element, but it is not sufficient to describe the structure of all giant planets. A description of the high-pressure behavior of other elements would go beyond the scope of the present review. We only sketch a few important results here.

In order to obtain tractable equations of state in the entire domain of pressure and temperature spanned by the planets during their evolution, one has to consider simplifications, among which the first one is to consider that an element (e.g., hydrogen) dominates, and that others can be considered as a perturbation. This is done for the hydrogen-helium mixture for the now classical EOS by Saumon et al. (1995), and now with more up-to-date EOSs (Caillabet et al., 2011; Nettelmann et al., 2012; Militzer and Hubbard, 2013). The addition of other elements can be done through the so-called additive volume rule which is generally a good approximation given other sources of uncertainty (Vorberger et al. (2007); see also Chabrier and Ashcroft (1990)).

Equations of state for elements other than hydrogen and helium in the parameter range relevant for giant planetary interiors have traditionally been difficult to obtain, and are often not easily shared. Beyond an extrapolation from the classical ANEOS and Sesame tables (see Saumon and Guillot, 2004, and references therein), new results have become available. In particular, ab-initio simulations revealed that when compressing water or ammonia along an isentrope from conditions relevant to the atmospheres of Uranus and Neptune, they transition from a molecular to a ionic fluid, then to a superionic fluid and finally to a plasma (Cavazzoni et al., 1999). The superionic fluid corresponds

to a state in which protons move relatively freely among a lattice of oxygen atoms. An equation of state for water has been calculated from first-principles by French et al. (2009) and is found to be in good agreement with experiments (Knudson et al., 2012). A similar equation of state for ammonia is presented by Bethkenhagen et al. (2013). In models of Uranus and Neptune, for water, the ionic transition occurs near 0.1 Mbar and the superionic transition near 1 Mbar (Redmer et al., 2011).

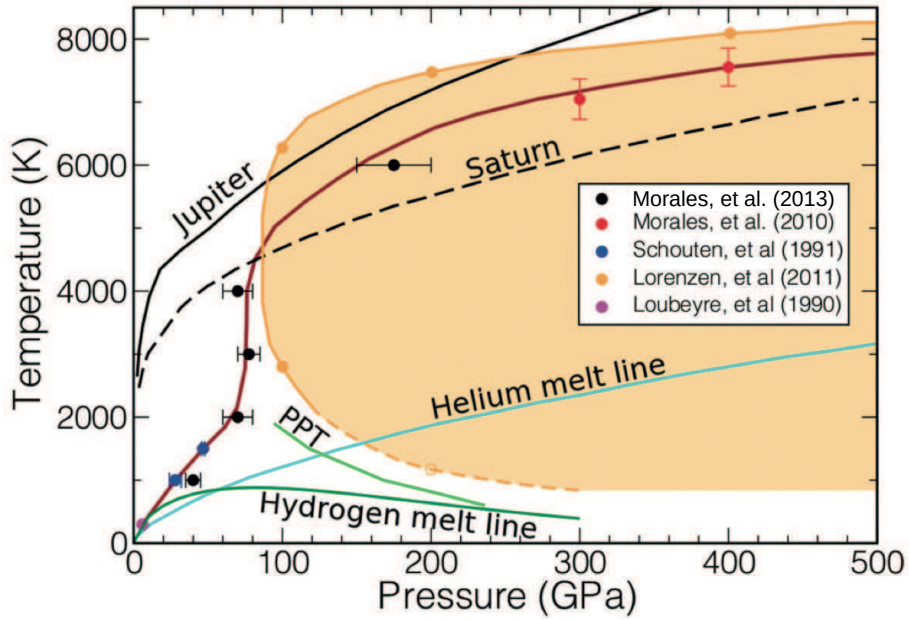

Figure 6. Phase diagram for the hydrogen-helium mixture for a helium mole concentration of 8%. The orange region shows where the two elements are expected to separate from each other according to the calculations of Lorenzen et al. (2011). The red curve correspond to the critical temperature for that separation according to Morales et al. (2013a). Numerical results by Schouten et al. (1991) and experimental determinations by Loubeyre et al. (1991) are also shown. The back curves show the isentropes of Jupiter (plain) and Saturn (dashed) respectively. [From Morales et al. (2013a)].

In some cases however, generally at low enough temperatures for a given pressure range, mixtures cannot remain homogeneous. This further complicates the calculation of equations of state and has important physical consequences for the planetary structure: the two components having different molecular weights, they tend to be separated by gravity so that the heavier component settles down under the lighter one. This is the case of the hydrogen and helium mixture for which it was proposed that such a separation would occur in Saturn already in the 1970s (Salpeter, 1973; Stevenson and Salpeter, 1977a), but for which realistic calculations have only become possible in the past decade or so (see Morales et al., 2009; Lorenzen et al., 2011; Morales et al., 2013a). Figure 6 shows the comparison between two of these calculations based on first-principles simulations. According to these calculations, Saturn's interior is in the phase separation region below 1 Mbar but whether Jupiter is too depends on which calculation is considered.

The separation of other mixtures have also been calculated and is relevant to understand the initial formation and subsequent possible erosion of the cores of giant planets (see Guillot et al., 2004). First-principles calculations of the water in metallic hydrogen (at pressures above 10 Mbar) predict a critical phase separation temperature of less than 4000 K (Wilson and Militzer, 2010) implying that water is completely soluble in hydrogen in the interiors of Jupiter, Saturn and generally gas giants. This is also the case of iron, with a critical temperature of around 2000 K (Wahl et al., 2013). Finally, mixing rocks (specifically MgO) and metallic hydrogen is also relatively easy, even though the critical temperature for the same pressure range is higher, of order 10,000 K or less (Wilson and Militzer, 2012).

3.3. Heat transport

Giant planets possess hot interiors, implying that a relatively large amount of energy has to be transported from the deep regions of the planets to their surface. This can either be done by radiation, conduction, or, if these processes are not sufficient, by convection. Convection is generally ensured by the rapid rise of the opacity with increasing pressure

and temperature. At pressures of a bar or more and relatively low temperatures (less than 1000 K), the three dominant sources of opacities are water, methane and collision-induced absorption by hydrogen molecules.

However, in the intermediate temperature range between ∼ 1200 and 1500 K, the Rosseland opacity due to the hydrogen and helium absorption behaves differently: the absorption at any given wavelength increases with density, but because the temperature also rises, the photons are emitted at shorter wavelengths, where the monochromatic absorption is smaller. As a consequence, the opacity can decrease. This was shown by Guillot et al. (1994) to potentially lead to the presence of a deep radiative zone in the interiors of Jupiter, Saturn and Uranus.

This problem must however be reanalyzed in the light of observations and analyses of brown dwarfs. Their spectra show unexpectedly wide sodium and potassium absorption lines (see Burrows, Marley & Sharp 2000), in spectral regions where hydrogen, helium, water, methane and ammonia are relatively transparent. It thus appears that the added contribution of these elements (if they are indeed present) would wipe out any radiative region at these levels (Guillot et al., 2004).

At temperatures above 1500 ∼ 2000 K two important sources of opacity appear: (i) the rising number of electrons greatly enhances the absorption of H_2^- and H^-; (ii) TiO, a very strong absorber at visible wavelengths is freed by the vaporization of $CaTiO_3$. Again, the opacity rises rapidly which ensures a convective transport of the heat. Still deeper, conduction by free electrons becomes more efficient, but the densities are found not to be high enough for this process to be significant, except perhaps near the central core (see Hubbard, 1968; Stevenson and Salpeter, 1977b).

While our giant planets seem to possess globally convective interiors, strongly irradiated extrasolar planets must develop a radiative zone just beneath the levels where most of the stellar irradiation is absorbed. Depending on the irradiation and characteristics of the planet, this zone may extend down to kbar levels, the deeper levels being convective. In this case, a careful determination of the opacities is necessary (but generally not possible) as these control the cooling and contraction of the deeper interior (see Freedman et al., 2008, for a discussion of opacities and tables for substellar atmospheres and interiors).

3.4. The contraction and cooling histories of giant planets

The interiors of giant planets are expected to evolve with time from a high entropy, high θ value, hot initial state to a low entropy, low θ, cold degenerate state. The essential underlying physics can be derived from the well-known virial theorem and the energy conservation which link the planet's internal energy E_i, gravitational energy E_g and luminosity through:

$$\xi E_\mathrm{i} + E_\mathrm{g} = 0, \tag{8}$$

$$L = -\frac{\xi - 1}{\xi}\frac{dE_\mathrm{g}}{dt}, \tag{9}$$

where $\xi = \int_0^M 3(P/\rho)dm / \int_0^M udm \approx <3P/\rho u>$, the brackets indicating averaging, and u is the specific internal energy. For a diatomic perfect gas, $\xi = 3.2$; for fully-degenerate non-relativistic electrons, $\xi = 2$.

Thus, for a giant planet or brown dwarf beginning its life mostly as a perfect H_2 gas, two third of the energy gained by contraction is radiated away, one third being used to increase E_i. The internal energy being proportional to the temperature, the effect is to heat up the planet. This represents the slightly counter-intuitive but well known effect that a star or giant planet initially heats up while radiating a significant luminosity (e.g., Kippenhahn and Weigert, 1994).

Let us now move further in the evolution, when the contraction has proceeded to a point where the electrons have become degenerate. For simplicity, we will ignore Coulomb interactions and exchange terms, and assume that the internal energy can be written as $E_\mathrm{i} = E_\mathrm{el} + E_\mathrm{ion}$, and that furthermore $E_\mathrm{el} \gg E_\mathrm{ion}$ (θ is small). Because $\xi \approx 2$, we know that half of the gravitational potential energy is radiated away and half of it goes into internal energy. The problem is to decide how this energy is split into an electronic and an ionic part. The gravitational energy changes with some average value of the interior density as $E_\mathrm{g} \propto 1/R \propto \rho^{1/3}$. The energy of the degenerate electrons is essentially the Fermi energy: $E_\mathrm{el} \propto \rho^{2/3}$. Therefore, $\dot{E}_\mathrm{g} \approx 2(E_\mathrm{g}/E_\mathrm{el})\dot{E}_\mathrm{el}$. Using the virial theorem and specifically eq. (8) we get that $\dot{E}_\mathrm{g} \approx -\dot{E}_\mathrm{el}$. The luminosity is by definition $L = -(\dot{E}_\mathrm{g} + \dot{E}_\mathrm{i})$ and therefore

$$L \approx -\dot{E}_\mathrm{ion} \propto -\dot{T}. \tag{10}$$

In this limit, the gravitational energy lost is entirely absorbed by the increase in pressure of the degenerate electrons and the observed luminosity is due to the thermal cooling of the ions (Guillot, 2005).

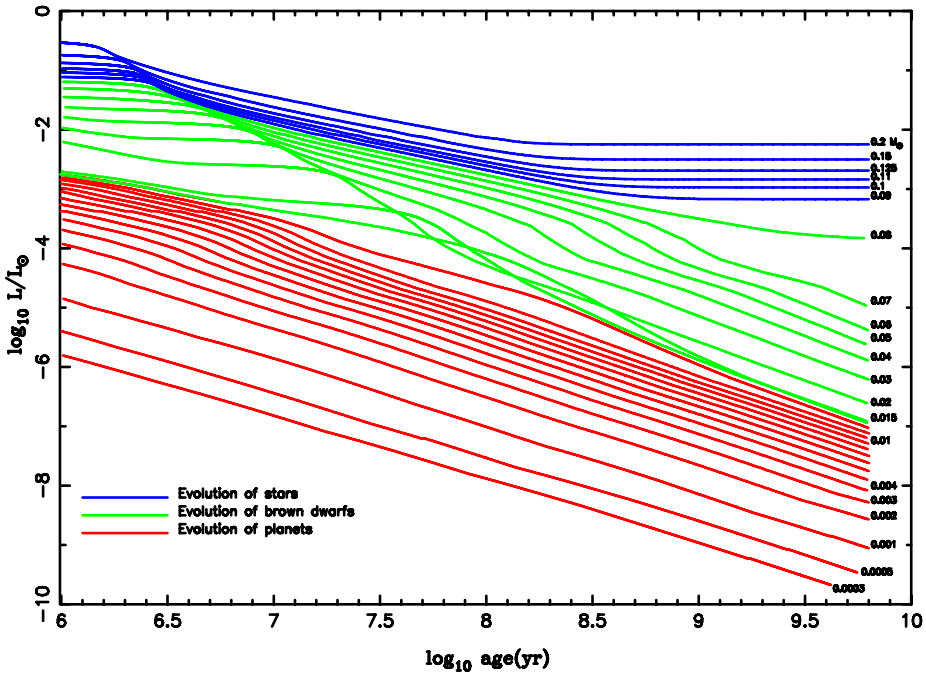

Figure 7. Evolution of the luminosity (in $L_\odot$) of solar-metallicity M dwarfs and substellar objects vs. time (in yr) after formation. In this figure, "brown dwarfs" are arbitrarily designated as those objects that burn deuterium, while those that do not are tentatively labelled "planets". Stars are objects massive enough to halt their contraction due to hydrogen fusion. Each curve is labelled by its corresponding mass in $M_\odot$, with the lowest three corresponding to the mass of Saturn, half the mass of Jupiter, and the mass of Jupiter. [From Burrows et al. (1997)].

Several simplifications limit the applicability of this result (that would be valid in the white dwarf regime). In particular, the Coulomb and exchange terms in the EOS introduce negative contributions that cannot be neglected. However, the approach is useful to grasp how the evolution proceeds: in its very early stages, the planet is very compressible. It follows a standard Kelvin-Helmholtz contraction. When degeneracy sets in, the compressibility becomes much smaller ($\alpha T \sim 0.1$, where α is the coefficient of thermal expansion), and the planet gets its luminosity mostly from the thermal cooling of the ions. The luminosity can be written in terms of a modified Kelvin-Helmholtz formula:

$$L \approx \eta \frac{GM^2}{R\tau}, \tag{11}$$

where τ is the age, and η is a factor that hides most of the complex physics. In the approximation that Coulomb and exchange terms can be neglected, $\eta \approx \theta/(\theta+1)$. The poor compressibility of giant planets in their mature evolution stages imply that $\eta \ll 1$ ($\eta \sim 0.03$ for Jupiter): the luminosity is not obtained from the entire gravitational potential, but from the much more limited reservoir constituted by the thermal internal energy. Equation (11) shows that to first order, $\log L \propto -\log \tau$: very little time is spent at high luminosity values. In other words, the problem is (in most cases) weakly sensitive to initial conditions. However, it is to be noticed that with progress in our capability to detect very young objects, i.e., planets and brown dwarfs of only a few million years of age, the problem of the initial conditions does become important (Marley et al., 2006). Interestingly, at these early stages, their luminosity appears to strongly depend on their core mass (Mordasini, 2013).

Figure 7 shows more generally how giant planets, but also brown dwarfs and small stars see their luminosities evolve as a function of time. The $1/\tau$ slope is globally conserved, with some variations for brown dwarfs during the transient epoch of deuterium burning, and of course for stars, when they begin burning efficiently their hydrogen and settle on the main sequence: in that case, the tendency of the star to contract under the action of gravity is exactly balanced by thermonuclear hydrogen fusion.

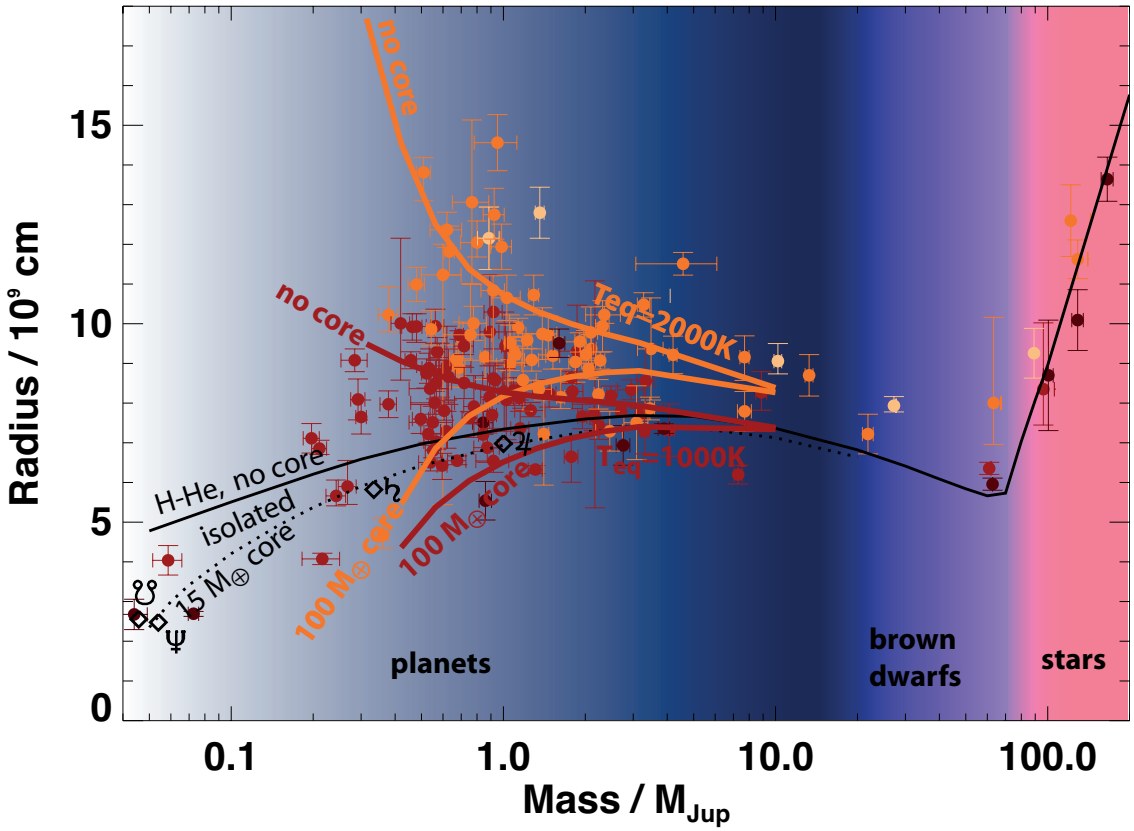

Figure 8. Theoretical and observed mass-radius relations. The black line is applicable to the evolution of solar composition planets, brown dwarfs and stars, when isolated or nearly isolated (as Jupiter, Saturn, Uranus and Neptune, defined by diamonds and their respective symbols), after 5 Ga of evolution. The dotted line shows the effect of a 15 $M_\oplus$ core on the mass-radius relation. Orange and yellow curves represent the mass-radius relations for heavily irradiated planets with equilibrium temperatures of 1000 and 2000 K, respectively, and assuming that 0.5% of the incoming stellar luminosity is dissipated at the center (see section 4.3). For each irradiation level, two cases are considered: a solar-composition planet with no core (top curve), and one with a 100 $M_\oplus$ central core (bottom curve). Circles with error bars correspond to known planets, brown dwarfs and low-mass stars, color-coded as a function of their equilibrium temperature(below 750, 1500, 2250 K and above 2250 K, respectively, from darkest to lightest).

3.5. Mass-radius relation

The relation between mass and radius has very fundamental astrophysical applications. Most importantly it allows one to infer the gross composition of an object from a measurement of its mass and radius. This is especially relevant in the context of the discovery of extrasolar planets with both radial velocimetry and the transit method, as the two techniques yield relatively accurate determination of M and R, these determinations being often limited by the uncertainty on the stellar parameters themselves.

Figure 8 shows mass-radius relations for compact degenerate objects from giant planets to brown dwarfs and low-mass stars. The right-hand side of the diagram shows a rapid increase of the radius with mass in the stellar regime which is directly due to the onset of stable thermonuclear reactions. In this regime, observations and theoretical models agree (see however Ribas, 2006, for a more detailed discussion). The left-hand side of the diagram is obviously more complex, and this can be understood by the fact that planets have much larger variations in composition than stars, and because external factors such as the amount of irradiation they receive do affect their contraction in a significant manner.

Let us first concentrate on isolated or nearly-isolated gaseous planets. The black curves have a local maximum near $4\,\mathrm{M_J}$: at small masses, the compression is small so that the radius increases with mass. At large masses, degeneracy sets in and the radius decreases with mass.

This can be understood on the basis of polytropic models based on the assumption that $P = K\rho^{1+1/n}$, where K and n are constants. Because of degeneracy, a planet of large mass will tend to have $n \to 1.5$, while a planet of smaller mass will be less compressible ($n \to 0$). Indeed, it can be shown that in their inner 70 to 80% in radius isolated solar composition planets of 10, 1 and $0.1\,\mathrm{M_J}$ have $n = 1.3$, 1.0 and 0.6, respectively. From polytropic equations (e.g., Chandrasekhar, 1939):

$$R \propto K^{\frac{n}{3-n}} M^{\frac{1-n}{3-n}}. \tag{12}$$

Assuming that K is independant of mass, one gets $R \propto M^{0.16}$, M^0, and $M^{-0.18}$ for $M = 10$, 1 and $0.1\,\mathrm{M_J}$, respectively, in relatively good agreement with fig. 8 (the small discrepancies are due to the fact that the intrinsic luminosity and hence K depend on the mass considered).

Figure 8 shows already that the planets in our Solar System are not made of pure hydrogen and helium and require an additional fraction of heavy elements in their interior, either in the form of a core, or distributed in the envelope (dotted line).

For extrasolar planets, the situation is complicated by the fact that the intense irradiation that they receive plays a major role in their evolution. The present sample is already quite diverse, with equilibrium temperature (defined as the effective temperature corresponding to the stellar flux received by the planet) ranging from 1000 to 2500 K. Their compositions are also quite variable, with some planets having large masses of heavy elements (Sato et al., 2005; Guillot et al., 2006). The orange and yellow curves in fig. 8 show theoretical results for equilibrium temperatures of 1000 and 2000 K, respectively. Two extreme models have been plotted: assuming a purely solar composition planet (top curve), and assuming the presence of a $100\,\mathrm{M_\oplus}$ central core (bottom curve). In each case, an additional energy source proportional to 0.5% of the incoming luminosity was also assumed (see discussion in § 4.3 hereafter).

The increase in radius for decreasing planetary mass for irradiated, solar-composition planets with little or no core can be understood using the polytropic relation (eq. 12), but accounting for variations of K as defined by the atmospheric boundary condition. Using the Eddington approximation, assuming $\kappa \propto P$ and a perfect gas relation in the atmosphere, one can show that $K \propto (M/R^2)^{-1/2n}$ and that therefore $R \propto M^{\frac{1/2-n}{2-n}}$. With $n = 1$, one finds $R \propto M^{-1/2}$. Strongly irradiated hydrogen-helium planets of small masses are hence expected to have the largest radii which qualitatively explain the positions of the extrasolar planets in fig. 8. Note that this estimate implicitly assumes that n is constant throughout the planet. The real situation is more complex because of the growth of a deep radiative region in most irradiated planets, and because of structural changes between the degenerate interior and the perfect gas atmosphere (Guillot, 2005).

In the case of the presence of a fixed mass of heavy elements, the trend is inverse because of the increase of mean molecular mass (or equivalently core/envelope mass) with decreasing total mass. Thus, small planets with a core are much more tightly bound and less subject to evaporation than those that have no core.

3.6. Rotation and the figures of planets

The mass and radius of a planet informs us on its global composition. Because planets are also rotating, one is allowed to obtain more information on their deep interior structure. The hydrostatic equation becomes more complex however:

$$\frac{\nabla P}{\rho} = \nabla\left(G\iiint\frac{\rho(\mathbf{r}')}{|\mathbf{r}-\mathbf{r}'|}d^3\mathbf{r}'\right) - \mathbf{\Omega}\times(\mathbf{\Omega}\times\mathbf{r}), \tag{13}$$

where $\mathbf{\Omega}$ is the rotation vector. The resolution of eq. (13) is a complex problem. It can however be somewhat simplified by assuming that $|\mathbf{\Omega}| \equiv \omega$ is such that the centrifugal force can be derived from a potential. The hydrostatic equilibrium then writes $\nabla P = \rho\nabla U$, and the *figure* of the rotating planet is then defined by the $U = constant$ level surface.

One can show (e.g., Zharkov and Trubitsyn, 1978) that the hydrostatic equation of a fluid planet can then be written in terms of the mean radius $\overline{r}$ (the radius of a sphere containing the same volume as that enclosed by the considered equipotential surface):

$$\frac{1}{\rho}\frac{\partial P}{\partial\overline{r}} = -\frac{Gm}{\overline{r}^2} + \frac{2}{3}\omega^2\overline{r} + \frac{GM}{\overline{R}^3}\overline{r}\varphi_\omega, \tag{14}$$

where M and $\overline{R}$ are the total mass and mean radius of the planet, and φ_ω is a slowly varying function of $\overline{r}$. (In the case of Jupiter, φ_ω varies from about 2×10^{-3} at the center to 4×10^{-3} at the surface.) Equations (5-7) remain the same with the hypothesis that the level surfaces for the pressure, temperature, and luminosity are equipotentials. The significance of rotation is measured by the ratio of the centrifugal acceleration to the gravity:

$$q = \frac{\omega^2 R_{\rm eq}^3}{GM}. \tag{15}$$

As discussed in section 2.2, in some cases, the external gravity field of a planet can be accurately measured in the form of gravitational moments J_k (with zero odd moments for a planet in hydrostatic equilibrium) that measure the departure from spherical symmetry. Together with the mass, this provides a constraint on the interior density profile (see Zharkov and Trubitsyn (1974) -see also chapters by Van Hoolst and Sohl & Schubert):

$$\begin{aligned} M &= \iiint\rho(r,\theta)d^3\tau, \\ J_{2i} &= -\frac{1}{MR_{\rm eq}^{2i}}\iiint\rho(r,\theta)r^{2i}P_{2i}(\cos\theta)d^3\tau, \end{aligned}$$

where $d\tau$ is a volume element and the integrals are performed over the entire volume of the planet.

Figure 9 shows how the different layers inside a planet contribute to the mass and the gravitational moments. The figure applies to Jupiter, but would remain relatively similar for other planets. Note however that in the case of Uranus and Neptune, the core is a sizable fraction of the total planet and contributes both to J_2 and J_4. Measured gravitational moments thus provide information on the external levels of a planet. It is only indirectly, through the constraints on the outer envelope that the presence of a central core can be infered. As a consequence, it is impossible to determine this core's state (liquid or solid), structure (differentiated, partially mixed with the envelope) and composition (rock, ice, helium...) from the gravity field data.

The Juno (Bolton, 2010) and Cassini Solstice (Spilker, 2012) missions are expected to yield considerable improvements in our determination of the gravity fields of Jupiter and Saturn, respectively. Because the theory of figures is limited by its expansion in terms of the rotation parameter q and because purely barotropic solutions are possible only in the limit of solid-body rotation and of pure rotation on cylinders, these high precision measurements will require new approaches to include rotation in planetary models (see Hubbard, 1999, 2013). Separately, these measurements will enable new constraints such as the determination of the planets' angular momentum through the measurement of the relativistic Lense-Thirring effect (Iorio, 2010) and the determination of their moment of inertia (Helled, 2011; Helled et al., 2011b). But probably the most important prospects lie in the possibility to couple measurements on gravity field, magnetic fields and wind speeds with combined tri-dimensional magnetohydrodynamical models (see sections 2.3 and 2.4).

For planets outside the solar system, although measuring their gravitational potential is presently beyond reach, an indirect measurement of the planets' Love number k_2 may be possible in systems of planets in which one is locked

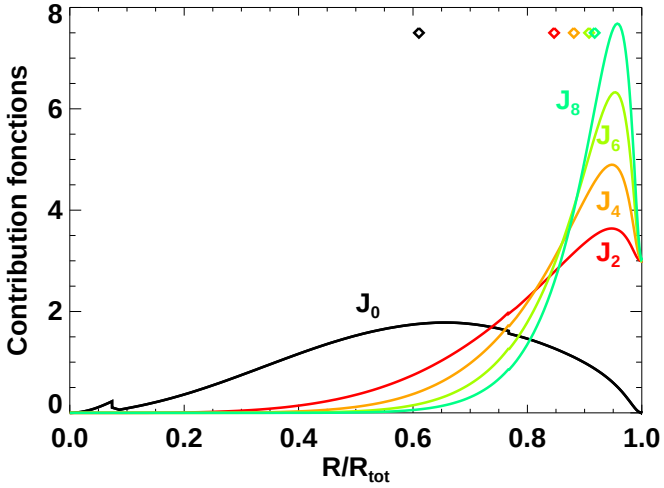

Figure 9. Contribution of the level radii to the gravitational moments of Jupiter. J_0 is equivalent to the planet's mass. The small discontinuities are caused by the following transitions, from left to right: core/envelope, helium rich/helium poor (metallic/molecular). Diamonds indicate the median radius for each moment. They correspond to pressures of 9.1, 1.3, 0.75, 0.45 and 0.35 Mbar, respectively, from left to right (J_0 to J_8).

into a so-called fixed-point eccentricity. So far, one such transiting system is known, HAT-P-13 (Batygin et al., 2009; Mardling, 2010), because it contains a transiting planet, HAT-P-13b and a companion, HAT-P-13c whose minimum mass $M \sin i$ and orbital eccentricity are known (Bakos et al., 2009). The value of k_2 constrains the interior structure in a way that is very similar to J_2 and has been used to obtain first constraints on the interior structure of this planet (Kramm et al., 2012).

4. Interior structures and evolutions

4.1. Jupiter and Saturn

As illustrated by fig. 10, the simplest interior models of Jupiter and Saturn matching all observational constraints assume the presence of three main layers: (i) an outer hydrogen-helium envelope, whose global composition is that of the deep atmosphere; (ii) an inner hydrogen-helium envelope, enriched in helium because the whole planet has to fit the H/He protosolar value; (iii) a central dense core. Because the planets are believed to be mostly convective, these regions are expected to be globally homogeneous. (Many interesting thermochemical transformations take place in the deep atmosphere, but they are of little concern to us).

The transition from a helium-poor upper envelope to a helium-rich lower envelope is thought to take place through the formation of helium-rich droplets that fall deeper into the planet due to their larger density. These droplets form when the temperature-pressure profiles enter the separation region for the initial helium abundance, as shown in section 3.2.2. Three-layer models implicitly make the hypothesis that this region is adiabatic (this is justified only if convection is not inhibited by the formation of helium droplets, as discussed by Stevenson and Salpeter (1977a)) and narrow. Figure 6 shows that this zone may be extended, especially in present-day Saturn (see also Fortney and Hubbard, 2003).

As discussed by Stevenson and Salpeter (1977a); Stevenson (1982) the planets would start from an initially hot and homogeneous state and would start entering the phase separation region progressively, leading to a depletion of helium in the outer region and its increase in the deeper interior. According to the calculations by Lorenzen et al. (2011) and Morales et al. (2013a) the separation would first occur at a pressure between 1 and 2 Mbar and the inhomogeneous region would grow inward but not so much towards lower pressures because of the higher solubility of helium in molecular hydrogen. According to the simulations, although needed to explain the abundances in Jupiter's atmosphere (section 2.6), it is not yet clear that the process has begun in this planet. Fully consistent calculations

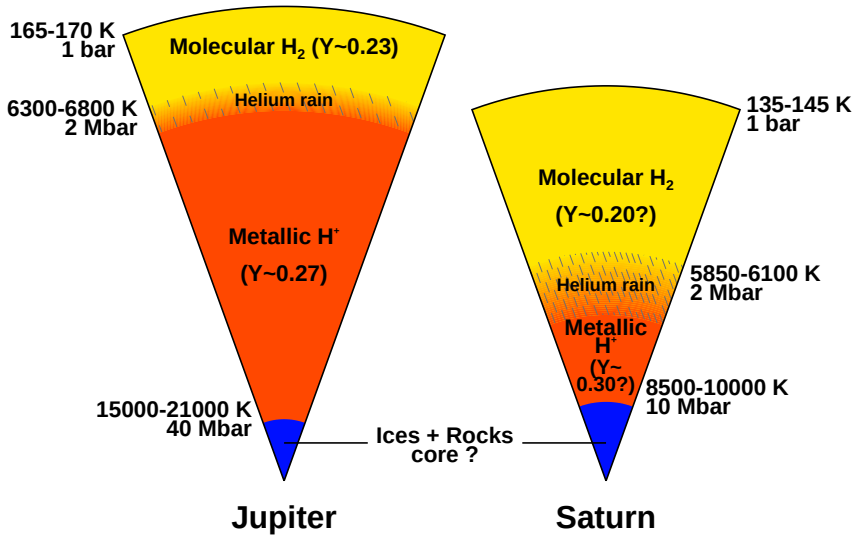

Figure 10. Schematic representation of the interiors of Jupiter and Saturn. The range of temperatures is estimated using homogeneous models and including a possible radiative zone indicated by the hashed regions. Helium mass mixing ratios Y are indicated. The size of the central rock and ice cores of Jupiter and Saturn is very uncertain (see text). In the case of Saturn, the inhomogeneous region may extend down all the way to the core which would imply the formation of a helium core. [Adapted from Guillot (1999b)].

that account both for the constraints on the planets' gravitational moments and their atmospheric composition should become possible, especially with the additional information brought by the Juno (Bolton, 2010) and Cassini Solstice (Spilker, 2012) space missions.

In the absence of these calculations, adiabatic three-layer models can be used as a useful guidance to a necessarily hypothetical ensemble of allowed structures and compositions of Jupiter and Saturn. A relatively extensive exploration of the parameter space has been performed by several authors (Saumon and Guillot, 2004; Fortney and Nettelmann, 2010; Nettelmann et al., 2012, 2013b; Helled and Guillot, 2013). The calculations account for a transition from a helium-poor outer envelope to a helium-rich inner envelope. The abundance of heavy elements may or may not be held constant across this transition. Many sources of uncertainties are taken into account however; among them, the most significant are on the equations of state of hydrogen and helium, the uncertain values of J_4 and J_6, the presence of differential rotation deep inside the planet, the location of the helium-poor to helium-rich region, and the uncertain helium to hydrogen protosolar ratio.

Their results indicate that Jupiter's core is smaller than $\sim 10\,M_\oplus$, and that its global composition is pretty much unknown (between 10 to $42\,M_\oplus$ of heavy elements in total). The models indicate that Jupiter is enriched compared to the solar value by a factor 1.5 to 8 times the solar value. This enrichment is compatible with a global uniform enrichment of all species near the atmospheric Galileo values, but allows many other possibilities as well.

Other models of Jupiter based on an ab-initio equation of state by (Militzer et al., 2008) led to a solution with a large core mass and a very small enrichment in heavy elements in the envelope incompatible with either the Galileo probe measurements or the protosolar helium abundance. A significant update in the EOS is presented by Militzer and Hubbard (2013). This updated EOS yields a warmer interior than the 2008 models and should therefore lead to a smaller core mass and larger amount of heavy elements in the envelope, in line with the other results. At the same time, the Militzer and Hubbard (2013) EOS is much more accurate than the range of EOSs used by Saumon and Guillot (2004) and it differs slightly from the other ab-initio EOS used by Nettelmann et al. (2012) and Nettelmann et al. (2013b). New constraints should therefore be derived on the basis of those new data.

In the case of Saturn, the solutions depend less on the hydrogen EOS because the Mbar pressure region is comparatively smaller. The total amount of heavy elements present in the planet can therefore be estimated with a better accuracy than for Jupiter, and is between 16 and $30\,M_\oplus$ (Nettelmann et al., 2013b; Helled and Guillot, 2013). The uncertainty on the core mass is found to be larger than for Jupiter because a heavy-element rich inner envelope can

mimic the gravitational signature of the core. As a result only an upper limit on the core mass of 20 $M_\oplus$ is derived.

Concerning the *evolutions* of Jupiter and Saturn, the three main sources of uncertainty are, by order of importance: (1) the magnitude of the helium separation; (2) the EOS; (3) the atmospheric boundary conditions. Figure 11 shows an ensemble of possibilities that attempts to bracket the minimum and maximum cooling. In all these quasi-adiabatic cases, helium sedimentation is needed to explain Saturn's present luminosity (see Salpeter, 1973; Stevenson and Salpeter, 1977a; Hubbard, 1977; Hubbard et al., 1999; Fortney and Hubbard, 2003). In the case of Jupiter, the sedimentation of helium that appears to be necessary to explain the low atmospheric helium abundance poses a problem for evolution models because it appears to generally prolong its evolution beyond 4.55 Ga, the age of the Solar System (Fortney et al., 2011; Nettelmann et al., 2012). However, different solutions are possible, including improvements of the EOS and atmospheric boundary conditions, or even the possible progressive erosion of the central core that would yield a lower luminosity of Jupiter at a given age (Guillot et al., 2004).

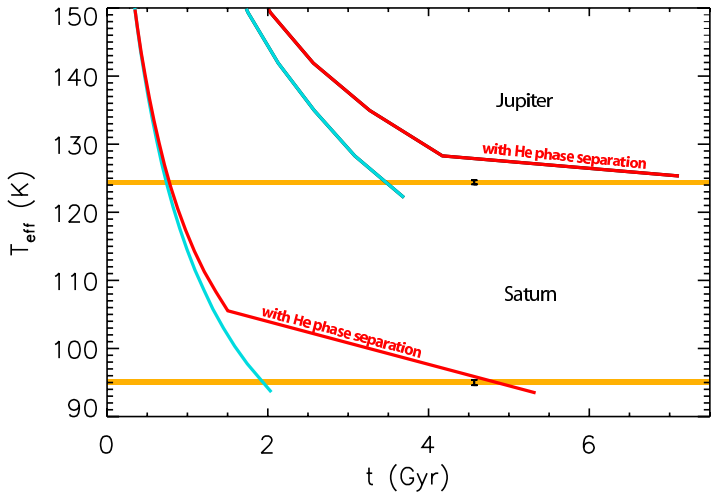

Figure 11. Final stages of evolution of Jupiter and Saturn. The present effective temperatures, reached after ~ 4.55 Ga of evolution, are indicated as horizontal orange lines. For each planet two models represent attempts to bracket the ensemble of possibilities, with the faster evolution corresponding to that of an homogeneous planet, while the slowest evolution includes the effect of helium settling in the last evolution phase. [Adapted from Hubbard et al. (1999) and Fortney and Hubbard (2003)].

A different set of solutions appears when one considers the possibility that the envelopes of Jupiter and Saturn are *not* homogeneous and adiabatic on large scales, but are instead of variable composition, with heavier elements at the bottom. In that case, convection can be strongly inhibited which requires the temperature gradient to be larger in order to transport the same intrinsic luminosity. In the case of giant planets, this process, known as semiconvection or diffusive convection leads to the formation of a non-static staircase structure with diffusive interfaces with abrupt variations of temperature and composition and a homogeneous adiabatic structure inbetween (Stevenson, 1985b; Rosenblum et al., 2011). By assuming that this structure is maintained over the entire envelopes of Jupiter and Saturn, Leconte and Chabrier (2012) derive much warmer interior structures with also 30% to 60% more heavy elements than in conventional models. However, the assumption that this non-homogenous composition is maintained in the entire envelopes is ad hoc. In reality, one may expect semi-convection to be confined to a much smaller region and thus have a more limited effect. The problem is open however and requires further study. Its understanding is also critical for deciding whether Jupiter's core can erode into its envelope (see Guillot et al., 2004; Wilson and Militzer, 2012).

As discussed in sections 2.3 and 2.4, classical interior models of Jupiter and Saturn based on the assumption of a homogeneous structure in the molecular envelope and an increase of the conductivity mainly due to hydrogen metallization do yield solutions for their magnetic fields and atmospheric zonal winds that globally match the observations. However, important "details" such as why Saturn's magnetic field is axisymmetric and Jupiter is not remain unexplained. Coupling interior and dynamical models in order to fit both Jupiter and Saturn's gravity and magnetic fields as well as their observed zonal winds (see sections 2.3 and 2.4) should bring a more global understanding of the planetary structures.

4.2. Uranus and Neptune

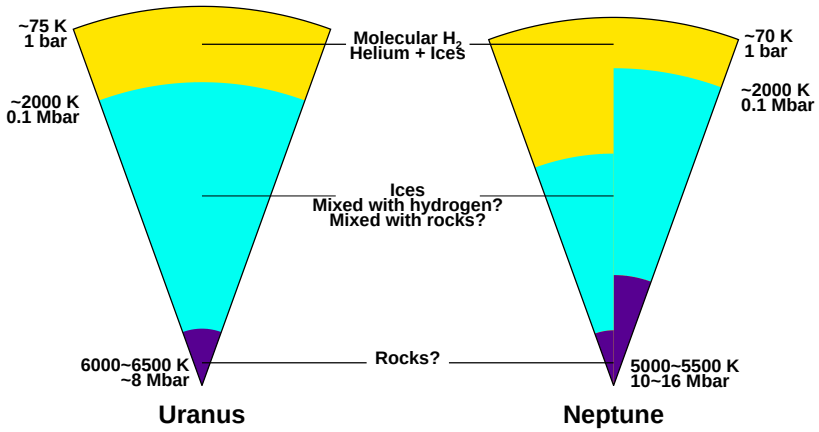

Figure 12. Schematic representation of the interiors of Uranus and Neptune. The ensemble of possibilities for Neptune is larger. Two possible structures are shown. [Adapted from Guillot (1999b) using results from Nettelmann et al. (2013a)].

Although the two planets are relatively similar, table 3 already shows that Neptune's larger mean density compared to Uranus has to be due to a slightly different composition: either more heavy elements compared to hydrogen and helium, or a larger rock/ice ratio. The gravitational moments impose that the density profiles lie close to that of "ices" (a mixture initially composed of e.g., H_2O, CH_4 and NH_3, but which rapidly becomes a ionic fluid of uncertain chemical composition in the planetary interior), except in the outermost layers, which have a density closer to that of hydrogen and helium (Marley et al., 1995; Podolak et al., 2000). As illustrated in fig. 12, three-layer models of Uranus and Neptune consisting of a central "rocks" core (magnesium-silicate and iron material), an ice layer and a hydrogen-helium gas envelope have been calculated (Podolak et al., 1991; Hubbard et al., 1995; Fortney and Nettelmann, 2010; Helled et al., 2011a; Nettelmann et al., 2013a).

According to the models of Nettelmann et al. (2013a), Uranus contains a minimum of 1.8 to 2.2 $M_\oplus$ of hydrogen and helium and Neptune 2.7 to 3.3 $M_\oplus$. The global ice to rock ratio that is derived is very high (19 to 36) in Uranus, while Neptune has a wide range of solutions from 3.6 to 14. These values are much larger than the canonical ice to rock ratio of 2 to 3 for the protosun that accounts for the abundances of all elements condensing at low temperatures ("ices") versus that of more refractory elements ("rocks"). The fact that either planet would have accreted much less rocks than ices is puzzling and unexplained by formation models. It is probably an artefact from assuming ices being confined to the envelope and rocks to the core.

The evolution of the two planets also remains a mystery. While Neptune's present luminosity may be explained by the adiabatic cooling of the planet over the age of the Solar System, this is not the case of Uranus's very low luminosity (Podolak et al., 1995; Fortney et al., 2011; Nettelmann et al., 2013a). This could be explained by the presence of a strongly inhibiting compositional gradient decoupling an inner region which would remain hot and an outer envelope which would cool progressively(Podolak et al., 1995). Such regions could also be present in Neptune but considerably deeper. Unfortunately, this qualitative explanation cannot be tied to the inferred interior structures. Apart from the latest models by (Nettelmann et al., 2013a), the models of Uranus and Neptune are too similar (and so are their magnetic fields – see section 2.3) to explain why Uranus would have such a small intrinsic heat flux and not Neptune.

In fact, it is likely that all present models of Uranus and Neptune are inadequate because of the assumption of an adiabatic temperature structure across interfaces with different compositions. Instead, diffusive-convection should occur and lead to strongly superadiabatic temperature gradient (e.g., Rosenblum et al., 2011). As in the case of Jupiter and Saturn (see Leconte and Chabrier, 2012), this would lead to higher temperatures in the interior and very different constraints on the interior composition. The amount of rocks required to fit the mean density and gravitational moments would certainly rise, potentially solving the ice to rock ratio problem. The evolution of the planets would

be very different as the present-day luminosity would be mostly governed by the leak of heat from the hot interior by diffusion at the interfaces.

4.3. Irradiated giant planets

4.3.1. Interior structure and dynamics

The physics that governs the calculation of interior structure and evolution models of giant planets described in the previous sections can be applied in principle to any gaseous exoplanet and brown dwarf. We focus the discussion on the ones that orbit extremely close to their star because of the possibility to directly characterise them and measure their mass, radius and in some cases even the properties of their atmosphere. Two planets are proxies for this new class of objects: the first extrasolar giant planet discovered, 51 Peg b, with an orbital period of $P = 4.23$ days, and the first *transiting* extrasolar giant planet, HD 209458 b, with $P = 3.52$ days. Following widespread usage, we call these planets "hot Jupiters" (a.k.a "Pegasids" since these two archetypes have been discovered in the Pegasus constellation).

With such a short orbital period, these planets are for most of them subject to an irradiation from their central star that is so intense that the absorbed stellar energy flux can be about $\sim 10^4$ times larger than their intrinsic flux. The atmosphere is thus prevented from cooling, with the consequence that a radiative zone develops and governs the cooling and contraction of the interior (Guillot et al., 1996). Typically, for a planet like HD 209458 b, this radiative zone extends to kbar levels, $T \sim 4000$ K, and is located in the outer 5% in radius (0.3% in mass) (Guillot and Showman, 2002).

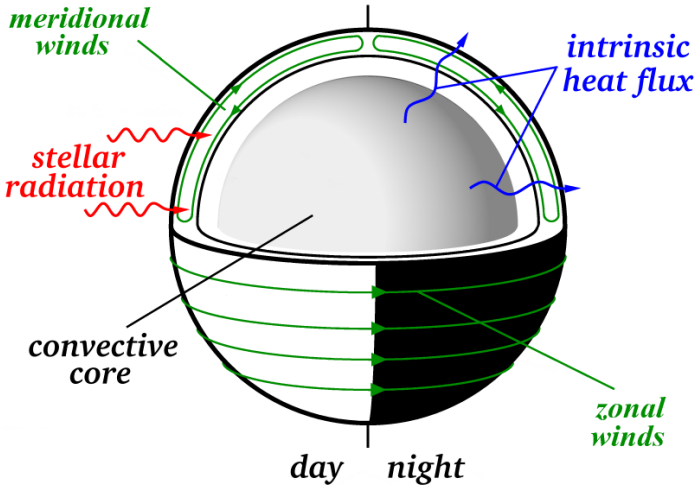

Figure 13. Conjectured dynamical structure of hot Jupiters (strongly irradiated extrasolar giant planets): At pressures larger than $0.1 - -1$ kbar, the intrinsic heat flux must be transported by convection. The convective core is at or near synchronous rotation with the star and has small latitudinal and longitudinal temperature variations. At lower pressures a radiative envelope is present. The top part of the atmosphere is penetrated by the stellar light on the day side. The spatial variation in insolation should drive winds that transport heat from the day side to the night side. [From Showman and Guillot (2002)].

Problems in modeling the evolution of hot Jupiters arise because of the uncertain outer boundary condition. The intense stellar flux implies that the atmospheric temperature profile is extremely dependent upon the opacity sources considered. Depending on the chosen composition, the opacity data used, the assumed presence of clouds, the geometry considered, resulting temperatures in the deep atmosphere can differ by up to ~ 600 K (Seager and Sasselov, 2000; Goukenleuque et al., 2000; Barman et al., 2001; Sudarsky et al., 2003; Iro et al., 2005; Fortney et al., 2006). Furthermore, as illustrated by fig. 13, the strong irradiation and expected synchronization of the planets' spin implies that strong inhomogeneities should exist in the atmosphere with in particular strong (~ 500 K) day-night and equator-

to-pole differences in effective temperatures (Showman and Guillot, 2002; Iro et al., 2005; Cooper and Showman, 2005; Barman et al., 2005).

Figure 14 illustrates the expected structure for the atmosphere of HD209458b from a modern, tri-dimensional global circulation model coupled with a one-dimensional radiative transfer algorithm (Parmentier et al., 2013). All the caveats concerning these overforced simulations discussed in section 2.4 of course also apply and add to the uncertainties stemming from the poorly known chemical composition. For example, the particular simulation of fig. 14 assumes the presence of TiO in the atmosphere, which yields very high temperatures at low pressures on the day side of the planet. It is not clear that this molecule is present or has condensed at deeper levels (see also Spiegel et al., 2009). Aside from that, the eastward equatorial circulation and the strong equator to pole gradient now appear to be a robust feature of these simulations (e.g., Showman and Guillot, 2002; Rauscher and Menou, 2013; Parmentier et al., 2013). As seen in fig. 14, the equatorial jet redistributes heat between the day side and the night side relatively efficiently at large pressures and on the equator, but this is not the case at the poles, and at low pressures, in line with the observational constraints (see section 2.10).

These strong temperature variations must influence at some point the cooling and contraction histories of hot Jupiters. When opacities variations are not included, they result in more loss of the intrinsic heat and a faster contraction than when assuming that the stellar irradiation is homogeneously redistributed across the planetary surface (Guillot and Showman, 2002; Guillot, 2010; Budaj et al., 2012; Spiegel and Burrows, 2013). However, given other uncertainties (e.g., on the chemical composition and opacities to be used), this has been neglected in planetary evolution models thus far.

4.3.2. Thermal evolution and inferred compositions

We have seen in fig. 8 that the measured masses and radii of transiting planets can be globally explained in the framework of an evolution model including the strong stellar irradiation and the presence of a variable mass of heavy elements, either in the form of a central core, or spread in the planet interior. However, when analyzing the situation for each planet, it appears that several planets are too large to be reproduced by standard models, i.e., models using the most up-to-date equations of state, opacities, atmospheric boundary conditions and assuming that the planetary luminosity governing its cooling is taken solely from the lost gravitational potential energy (see section 3.4).

Figure 15 illustrates the situation for the particular case of HD209458b: unless using an unrealistically hot atmosphere, or arbitrarily increasing the internal opacity, or decreasing the helium content, one cannot reproduce the observed radius which is 10 to 20% larger than calculated using standard models (Bodenheimer et al., 2001, 2003; Guillot and Showman, 2002; Baraffe et al., 2003). The fact that the measured radius corresponds to a low-pressure (∼mbar) level while the calculated radius corresponds to a level near 1 bar is not negligible (Burrows et al., 2003) but too small to account for the difference. This is problematic because while it is easy to invoke the presence of a massive core to explain the small size of a planet, a large size such as that of HD209458b requires an additional energy source, or significant modifications in the data/physics involved.

The discovery of many transiting hot Jupiters has shown that this phenomenon is widespread, with at least a third of them being oversized compared to predictions from the standard evolution of a solar-composition planet with no core (Guillot et al., 2006; Guillot, 2008; Laughlin et al., 2011). Numerous explanations have been put forward to explain this large size. The first ones, invoking tidal dissipation of eccentricity (Bodenheimer et al., 2001) or inclination (Winn and Holman, 2005) imply that orbital energy is transfered to the planet. These are generally too short-lived (e.g., Leconte et al., 2010) or of a low probability of occurrence (Levrard et al., 2007). The second ones posit that part of the irradiation energy is transferred into kinetic energy and is then dissipated deeper into the planet. This is the case of weather-noise (Showman and Guillot, 2002), ohmic dissipation (Batygin and Stevenson, 2010), thermal tides (Arras and Socrates, 2010) and turbulent burial (Youdin and Mitchell, 2010) models. These mechanisms appear quite promising as they are long-lived and generally require only a small fraction of order 1% or less of the irradiation luminosity to be transported and dissipated at deeper levels to explain the observed planets (Guillot and Showman, 2002). Finally, a third class of models is based on a reduced cooling, either through an ad hoc increase of opacities (Burrows et al., 2007) or inefficient heat transport due to semi-convection (Chabrier and Baraffe, 2007). Validating these models is becoming possible thanks to a large number of planets allowing statistical tests (see Laughlin et al., 2011), but will require further work.

In any case, the fact that a large number of planets are oversized lends weight to a mechanism that would apply to each planet. Masses of heavy elements can then be derived by imposing that all planets should be fitted by the

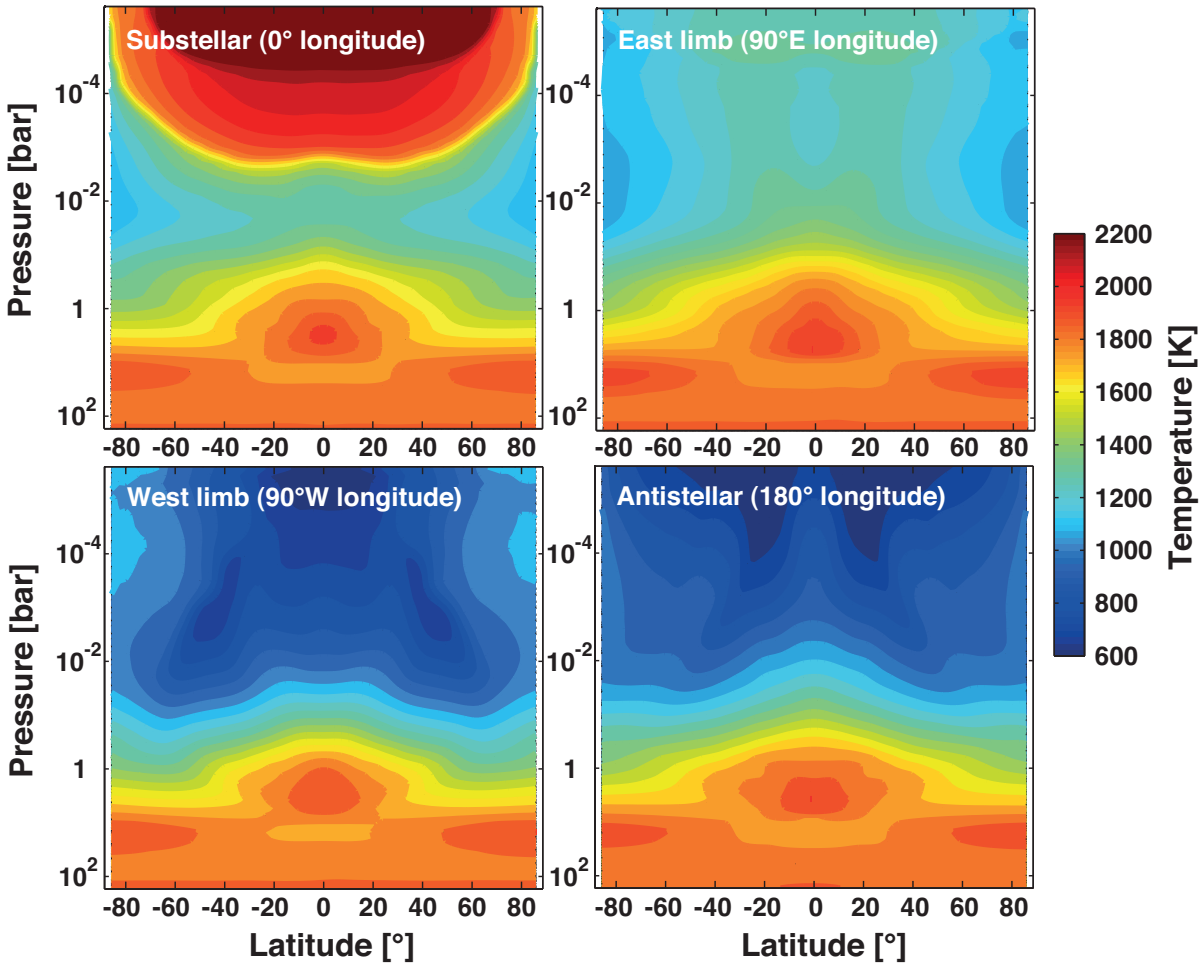

Figure 14. Simulated temperatures as a function of latitude (0° at the equator, ±90° at the poles) and pressure for HD209458 b obtained from a global 3D global circulation model. The four panels correspond to cuts from pole to pole at different longitudes (clockwise from the upper left): 0° (crossing the substellar point), 90°E (along the east limb), 180°E (crossing the antistellar point) and 270°E (along the west limb). A superrotating equatorial jet (0° latitude) is present and characterized by warmer temperatures than its surrounding at pressures of a few bars. The globally west to east circulation is responsible for a pronounced asymmetry between the warmer east limb and colder west limb. [Figure based on Parmentier et al. (2013). Courtesy of V. Parmentier.]

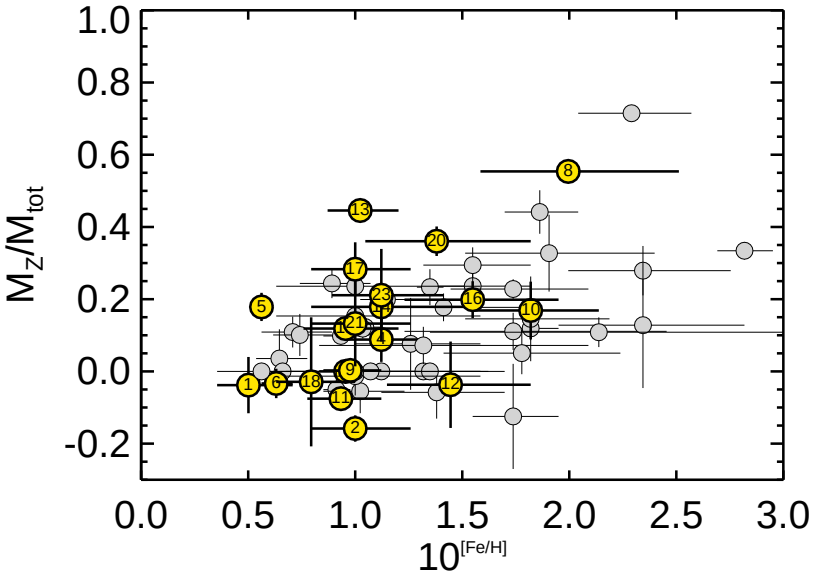

Figure 15. The contraction of HD209458b as a function of time can be compared to its measured radius and inferred age shown by the black box. Standard models (blue curve) for the evolution of that 0.69 M_J planet generally yield a radius that is too small compared to the observations, even for a solar composition and no central core (a larger core and -in most cases- larger amounts of heavy elements in the planet imply an even smaller size for a given age). Unrealistically low helium abundances or high opacities models lead to evolution tracks that barely cross the observational box. A possibility is that heat is dissipated into the deep interior by stellar tides, either related to a non-zero orbital eccentricity forced by an unseen companion, or because of a constant transfer of angular momentum from the heated atmosphere to the interior (black curve). Alternatively, the atmosphere may be hotter than predicted due to heating by strong zonal winds and shear instabilities (red curve).

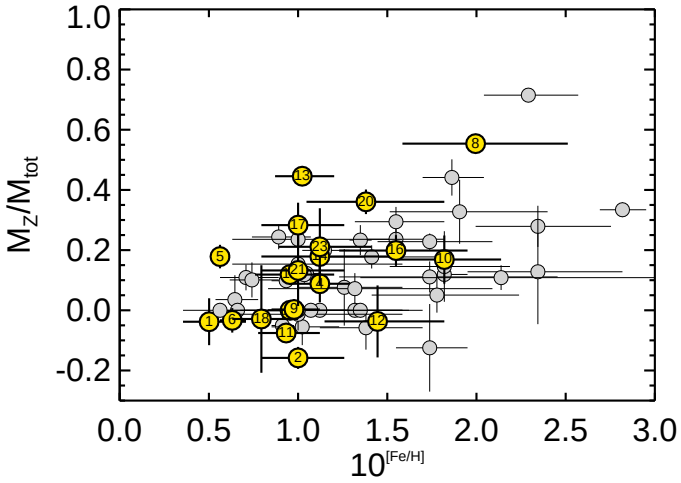

Figure 16. Mass fraction of heavy elements in the planets as a function of the metal content of their parent star expressed in solar units (e.g., $10^{[Fe/H]} = 3$ implies that the star contains three times more iron than our Sun). The evolution model assumes that 0.25% of the incoming irradiation flux is dissipated at the planet's center. Circles which are labeled 1 to 23 correspond to the CoRoT giant planets. Gray symbols correspond to a subset of known transiting systems (Guillot, 2008; Laughlin et al., 2011). Unphysical negative values for M_Z correspond to insufficient heat sources leading to a radius that is larger than observed. [From Moutou et al. (2013).]

same model with the same hypotheses. This can be done by inverting the results of fig. 8, as proposed by Guillot et al. (2006). On the basis of this hypothesis, figure 16 shows that some of the hot Jupiters contain a large fraction of heavy elements in their interior and that this fraction is correlated with the metallicity of the parent star. The large fraction of heavy elements is inferred both for relatively small giant planets (i.e., Saturn mass) and for planets which are several times the mass of Jupiter. A typical archetype of the first is HD149026 b which must contain around 70 $M_\oplus$ of heavy elements, a conclusion that is hard to escape because of the low total mass and high irradiation of the planet (see Ikoma et al., 2006; Fortney et al., 2006). For the latter, CoRoT-20b appears to push the models to the limit, with predicted masses of heavy elements in excess of 400 $M_\oplus$ (Deleuil et al., 2012).

The correlation between mass of heavy elements in hot Jupiters and stellar metallicity first obtained by Guillot et al. (2006) appears to stand the trial of time (Burrows et al., 2007; Guillot, 2008; Laughlin et al., 2011; Moutou et al., 2013), and remains valid when applied to planets with low irradiation levels which do not require additional physics to explain their large sizes (Miller and Fortney, 2011). It is important to realize that simply accreting slightly more metal-rich gas with the composition of the parent star would lead to a much smaller increase of a few percent at most. This correlation requires an efficient mechanism to collect solids in the protoplanetary disk and bring them into the hot Jupiters, something that is just beginning to be included into planet formation models (Mordasini et al., 2012).

Another intriguing possibility concerning hot Jupiters is that of a sustained mass loss due to the high irradiation dose that the planets receive. Indeed, this effect was predicted (Burrows and Lunine, 1995; Guillot et al., 1996; Lammer et al., 2003) and detected (Vidal-Madjar et al., 2003; Fossati et al., 2010; Bourrier et al., 2013). While its magnitude is still uncertain, it appears to have sculpted the population of planets in very close orbits around their star (e.g., Lopez et al., 2012).

The harvest of the Kepler and CoRoT missions opens the possibility to extend these studies to smaller planets. These objects are especially interesting but pose difficult problems in terms of structure because depending on their formation history, precise composition and location, they may be fluid, solid, or they may even possess a global liquid ocean (see Kuchner, 2003; Léger et al., 2004).

5. Implications for planetary formation models

The giant planets in our Solar System have in common a large mass of hydrogen and helium, but they are obviously quite different in their appearances, compositions and internal structures. Although studies cannot be conducted with the same level of details, we can safely conclude that extrasolar planets show a greater variety of compositions and structures, and imagine that their appearances differ even more significantly.

A parallel study of the structures of our giant planets and of giant planets orbiting around other stars should provide us with key information regarding planet formation in the next decade or so. But, already, some conclusions, some of them robust, others still tentative, can be drawn:

Giant planets formed in circumstellar disks, before these were completely dissipated:
This is a relatively obvious consequence of the fact that giant planets are mostly made of hydrogen and helium: these elements had to be acquired when they were still present in the disk. Because the observed lifetime of gaseous circumstellar disks is of the order of a few million years, this implies that these planets formed (i.e., acquired most of their final masses) in a few million years also, quite faster than terrestrial planets in the Solar System.

Giant planets migrated:
The observed orbital distribution of extrasolar planets and the presence of planets extremely close to their star is generally taken a strong evidence for an inward migration of planets, and various mechanisms have been proposed for that (see Ida and Lin, 2004a; Alibert et al., 2005; Moorhead and Adams, 2005, ...etc.). Separately, it was shown that several properties of our Solar System can be explained if Jupiter, Saturn, Uranus and Neptune ended the early formation phase in the presence of a disk with quasi-circular orbit, and with Saturn, Uranus and Neptune significantly closer to the Sun than they are now, and that these three planets subsequently migrated outward (Tsiganis et al., 2005).

Accretion played a key role for giant planet formation:
Although formation by direct gas instability still remains a possibility (e.g., Helled and Bodenheimer, 2011; Boley et al., 2011), several indications point towards a formation of giant planets that is dominated by accretion of heavy elements: First, Jupiter, Saturn, Uranus and Neptune are all significantly enriched in heavy elements compared to the Sun. This feature can be reproduced by core-accretion models, for Jupiter and Saturn at least (Alibert et al., 2005).

Second, the probability to find a giant planet around a solar-type star (with stellar type F, G or K) is a strongly rising function of stellar metallicity (Gonzalez, 1998; Santos et al., 2004; Fischer and Valenti, 2005), a property that is also well-reproduced by standard core accretion models (Ida and Lin, 2004b; Alibert et al., 2005). Third, the large masses of heavy elements inferred in some transiting extrasolar planets as well as the apparent correlation between mass of heavy elements in the planet and stellar metallicity (Guillot et al., 2006; Burrows et al., 2007; Guillot, 2008; Laughlin et al., 2011) is a strong indication that accretion was possible and that it was furthermore efficient.

Giant planets were enriched in heavy elements by core accretion, planetesimal delivery and/or formation in an enriched protoplanetary disk:
The giant planets in our Solar System are unambigously enriched in heavy elements compared to the Sun, both globally, and when considering their atmosphere. This may also be the case of extrasolar planets, although the evidence is still tenuous. The accretion of a central core can explain part of the global enrichment, but not that of the atmosphere. The accretion of planetesimals may be a possible solution but in the case of Jupiter at least the rapid drop in accretion efficiency as the planet reaches appreciable masses ($\sim 100\,M_\oplus$ or so) implies that such an enrichment would have originally concerned only very deep layers, and would require a relatively efficient upper mixing of these elements, and possibly an erosion of the central core (Guillot et al., 2004; Wilson and Militzer, 2012).

Although not unambiguously explained, the fact that Jupiter is also enriched in noble gases compared to the Sun is a key observation to understand some of the processes occuring in the early Solar System. Indeed, noble gases are trapped into solids only at very low temperatures, and this tells us either that most of the solids that formed Jupiter were formed at very low temperature to be able to trap gases such as argon, probably as clathrates (Gautier et al., 2001; Hersant et al., 2004; Mousis et al., 2012), or that the planet formed in an enriched disk as it was being evaporated (Guillot and Hueso, 2006). The fact that in Jupiter, argon, krypton and xenon have a comparable enrichment over the solar value within the error bars (see Lodders, 2008, and table 3) slightly favors the latter explanation.

6. Future prospects

We have shown that the compositions and structures of giant planets remain very uncertain. This is an important problem when attempting to understand and constrain the formation of planets, and the origins of the Solar System. However, the parallel study of giant planets in our Solar System by space missions such as Galileo and Cassini, and of extrasolar planets by both ground based and space programs has led to rapid improvements in the field, with in particular a precise determination of the composition of Jupiter's troposphere, and constraints on the compositions of a dozen of extrasolar planets.

Improvements on our knowledge of the giant planets requires a variety of efforts. Fortunately, nearly all of these are addressed at least partially by adequate projects in the next few years. The efforts that are necessary thus include (but are not limited to):

- Continue progresses on EOSs in order to obtain reliable results that can be used for a wide range of temperatures and pressures in the astrophysical context. This should be done with the help of laboratory experiments, for instance by using powerful lasers such as the NIF in the USA and the MégaJoule laser in France. Extensive numerical calculations should be performed as well, in particular with mixtures of elements.

- Calculate phase diagrams for a variety of mixtures, in particular involving superionic water, rocks, iron (and hydrogen). The hydrogen-helium phase diagram should also be refined because it is critical to understand the evolution and structure of Jupiter and Saturn.

- Have a better yardstick to measure solar and protosolar compositions. This has not been fully addressed by the Genesis mission and may require another mission and/or progresses in modeling the Sun's composition.

- Improve the measurement of Jupiter's gravity and magnetic fields, and determine the abundance of water in the deep atmosphere. This will be done by the Juno mission (Bolton, 2010) which is to arrive at Jupiter in 2016, and whose polar orbit skimming a mere 5000 km above the cloud tops should enable exquisite measurements of these quantities.

- Measure with high precision Saturn's gravity field. Saturn's gravitational moments have already been improved, but an important increase in accuracy can be obtained as part of the Cassini Solstice mission (Spilker, 2012), while the spacecraft plunges onto the planet. This should lead to better constraints, and possibly a determination of whether the interior of Saturn rotates as a solid body.

- Pursue the discovery of transiting extrasolar planets including some with longer orbital periods and around bright stars. A large number of these objects will enable detailed statistical studies which will be key in understanding this population of objects.

- Develop consistent models for the formation, evolution, present structure and magnetic field of Uranus and Neptune, in order to understand ice giants as a class of planets.

- It would be highly desirable to send a probe similar to the Galileo probe into Saturn's atmosphere (e.g., Marty et al., 2009). The comparison of the abundance of noble gases would discriminate between different models of the enrichment of the giant planets, and the additional measurement of key isotopic ratio would provide further tests to understand our origins.

- In the long term, a mission to the ice giants Uranus or Neptune would bring new views of these fascinating planets and help to complete our knowledge of the outer solar system.

Clearly, there is a lot of work on the road, but the prospects for a much improved knowledge of giant planets and their formation are bright.

Acknowledgements

The manuscript improved significantly thanks to the insightful reviews of Nadine Nettelmann and another reviewer. The authors also wish to thank Vivien Parmentier, Leigh Fletcher, Didier Saumon, Emmanuel Lellouch, Paul Loubeyre, Ravit Helled, Bill Hubbard, Erich Karkoschka, Imke De Pater and Miguel Morales for very useful comments and suggestions.

References

Acuna, M. H., Connerney, J. E. P., Ness, N. F., Nov. 1983. The Z3 zonal harmonic model of Saturn's magnetic field Analyses and implications. JGR88, 8771–8778.

Alibert, Y., Mordasini, C., Benz, W., Winisdoerffer, C., Apr. 2005. Models of giant planet formation with migration and disc evolution. A&A434, 343–353.

Anderson, J. D., Campbell, J. K., Jacobson, R. A., Sweetnam, D. N., Taylor, A. H., Dec. 1987. Radio science with Voyager 2 at Uranus - Results on masses and densities of the planet and five principal satellites. JGR92, 14877–14883.

Anderson, J. D., Schubert, G., Sep. 2007. Saturn's Gravitational Field, Internal Rotation, and Interior Structure. Science 317, 1384–.

Arras, P., Socrates, A., May 2010. Thermal Tides in Fluid Extrasolar Planets. ApJ714, 1–12.

Atreya, S. K., Mahaffy, P. R., Niemann, H. B., Wong, M. H., Owen, T. C., Feb. 2003. Composition and origin of the atmosphere of Jupiter - an update, and implications for the extrasolar giant planets. Plan. Space Sci.51, 105–112.

Bahcall, J. N., Pinsonneault, M. H., Wasserburg, G. J., Oct. 1995. Solar models with helium and heavy-element diffusion. Reviews of Modern Physics 67, 781–808.

Baines, K. H., Smith, H. W., May 1990. The atmospheric structure and dynamical properties of Neptune derived from ground-based and IUE spectrophotometry. Icarus85, 65–108.

Bakos, G. Á., Howard, A. W., Noyes, R. W., Hartman, J., Torres, G., Kovács, G., Fischer, D. A., Latham, D. W., Johnson, J. A., Marcy, G. W., Sasselov, D. D., Stefanik, R. P., Sipőcz, B., Kovács, G., Esquerdo, G. A., Pál, A., Lázár, J., Papp, I., Sári, P., Dec. 2009. HAT-P-13b,c: A Transiting Hot Jupiter with a Massive Outer Companion on an Eccentric Orbit. ApJ707, 446–456.

Baraffe, I., Chabrier, G., Barman, T. S., Allard, F., Hauschildt, P. H., May 2003. Evolutionary models for cool brown dwarfs and extrasolar giant planets. The case of HD 209458. A&A402, 701–712.

Baraffe, I., Chabrier, G., Barman, T. S., Selsis, F., Allard, F., Hauschildt, P. H., Jun. 2005. Hot-Jupiters and hot-Neptunes: A common origin? A&A436, L47–L51.

Barman, T. S., Hauschildt, P. H., Allard, F., Aug. 2001. Irradiated Planets. ApJ556, 885–895.

Barman, T. S., Hauschildt, P. H., Allard, F., Oct. 2005. Phase-Dependent Properties of Extrasolar Planet Atmospheres. ApJ632, 1132–1139.

Batygin, K., Bodenheimer, P., Laughlin, G., Oct. 2009. Determination of the Interior Structure of Transiting Planets in Multiple-Planet Systems. ApJL704, L49–L53.

Batygin, K., Stevenson, D. J., May 2010. Inflating Hot Jupiters with Ohmic Dissipation. ApJL714, L238–L243.

Bercovici, D., Schubert, G., Mar. 1987. Jovian seismology. Icarus69, 557–565.

Bethkenhagen, M., French, M., Redmer, R., Jun. 2013. Equation of state and phase diagram of ammonia at high pressures from ab initio simulations. Jour. Chem. Phys.138 (23), 234504.
Bodenheimer, P., Laughlin, G., Lin, D. N. C., Jul. 2003. On the Radii of Extrasolar Giant Planets. ApJ592, 555–563.
Bodenheimer, P., Lin, D. N. C., Mardling, R. A., Feb. 2001. On the Tidal Inflation of Short-Period Extrasolar Planets. ApJ548, 466–472.
Boley, A. C., Helled, R., Payne, M. J., Jul. 2011. The Heavy-element Composition of Disk Instability Planets Can Range from Sub- to Super-nebular. ApJ735, 30.
Bolton, S. J., Jan. 2010. The Juno Mission. In: Barbieri, C., Chakrabarti, S., Coradini, M., Lazzarin, M. (Eds.), IAU Symposium. Vol. 269 of IAU Symposium. pp. 92–100.
Bonev, S. A., Militzer, B., Galli, G., Jan. 2004. Ab initio simulations of dense liquid deuterium: Comparison with gas-gun shock-wave experiments. Phys. Rev. B69 (1), 014101–+.
Boriskov, G. V., Bykov, A. I., Il'Kaev, R. I., Selemir, V. D., Simakov, G. V., Trunin, R. F., Urlin, V. D., Shuikin, A. N., Nellis, W. J., Mar. 2005. Shock compression of liquid deuterium up to 109 GPa. Phys. Rev. B71 (9), 092104.
Borysow, A., Jorgensen, U. G., Zheng, C., Aug. 1997. Model atmospheres of cool, low-metallicity stars: the importance of collision-induced absorption. A&A324, 185–195.
Bouchy, F., Deleuil, M., Guillot, T., Aigrain, S., Carone, L., Cochran, W. D., Almenara, J. M., Alonso, R., Auvergne, M., Baglin, A., Barge, P., Bonomo, A. S., Bordé, P., Csizmadia, S., de Bondt, K., Deeg, H. J., Díaz, R. F., Dvorak, R., Endl, M., Erikson, A., Ferraz-Mello, S., Fridlund, M., Gandolfi, D., Gazzano, J. C., Gibson, N., Gillon, M., Guenther, E., Hatzes, A., Havel, M., Hébrard, G., Jorda, L., Léger, A., Lovis, C., Llebaria, A., Lammer, H., MacQueen, P. J., Mazeh, T., Moutou, C., Ofir, A., Ollivier, M., Parviainen, H., Pätzold, M., Queloz, D., Rauer, H., Rouan, D., Santerne, A., Schneider, J., Tingley, B., Wuchterl, G., Jan. 2011. Transiting exoplanets from the CoRoT space mission. XV. CoRoT-15b: a brown-dwarf transiting companion. A&A525, A68.
Bourrier, V., Lecavelier des Etangs, A., Dupuy, H., Ehrenreich, D., Vidal-Madjar, A., Hébrard, G., Ballester, G. E., Désert, J.-M., Ferlet, R., Sing, D. K., Wheatley, P. J., Mar. 2013. Atmospheric escape from HD 189733b observed in H I Lyman-α: detailed analysis of HST/STIS September 2011 observations. A&A551, A63.
Briggs, F. H., Sackett, P. D., Jul. 1989. Radio observations of Saturn as a probe of its atmosphere and cloud structure. Icarus 80, 77–103.
Budaj, J., Hubeny, I., Burrows, A., Jan. 2012. Day and night side core cooling of a strongly irradiated giant planet. A&A537, A115.
Burrows, A., Dec. 2013. Spectra as Windows into Exoplanet Atmospheres. ArXiv e-prints.
Burrows, A., Guillot, T., Hubbard, W. B., Marley, M. S., Saumon, D., Lunine, J. I., Sudarsky, D., May 2000. On the Radii of Close-in Giant Planets. ApJL534, L97–L100.
Burrows, A., Hubeny, I., Budaj, J., Hubbard, W. B., May 2007. Possible Solutions to the Radius Anomalies of Transiting Giant Planets. ApJ661, 502–514.
Burrows, A., Lunine, J., Nov. 1995. Extrasolar Planets - Astronomical Questions of Origin and Survival. Nature378, 333–+.
Burrows, A., Marley, M., Hubbard, W. B., Lunine, J. I., Guillot, T., Saumon, D., Freedman, R., Sudarsky, D., Sharp, C., Dec. 1997. A Nongray Theory of Extrasolar Giant Planets and Brown Dwarfs. ApJ491, 856–+.
Burrows, A., Sudarsky, D., Hubbard, W. B., Sep. 2003. A Theory for the Radius of the Transiting Giant Planet HD 209458b. ApJ594, 545–551.
Busse, F. H., 1978. Magnetohydrodynamics of the Earth's Dynamo. Annual Review of Fluid Mechanics 10, 435–462.
Caillabet, L., Mazevet, S., Loubeyre, P., Mar. 2011. Multiphase equation of state of hydrogen from ab initio calculations in the range 0.2 to 5 g/cc up to 10 eV. Phys. Rev. B83 (9), 094101.
Campbell, J. K., Synnott, S. P., Feb. 1985. Gravity field of the Jovian system from Pioneer and Voyager tracking data. AJ90, 364–372.
Cavazzoni, C., Chiarotti, G. L., Scandolo, S., Tosatti, E., Bernasconi, M., Parrinello, M., Jan. 1999. Superionic and Metallic States of Water and Ammonia at Giant Planet Conditions. Science 283, 44.
Cecconi, B., Zarka, P., Dec. 2005. Model of a variable radio period for Saturn. Journal of Geophysical Research (Space Physics) 110, 12203–+.
Chabrier, G., Ashcroft, N. W., Aug. 1990. Linear mixing rule in screened binary ionic mixtures. Phys. Rev. A42, 2284–2291.
Chabrier, G., Baraffe, I., May 2007. Heat Transport in Giant (Exo)planets: A New Perspective. ApJL661, L81–L84.
Chabrier, G., Saumon, D., Winisdoerffer, C., Jan. 2007. Hydrogen and Helium at High Density and Astrophysical Implications. Ap&SS307, 263–267.
Chandrasekhar, S., 1939. An introduction to the study of stellar structure. Chicago, Ill., The University of Chicago press [1939].
Charbonneau, D., Brown, T. M., Noyes, R. W., Gilliland, R. L., Mar. 2002. Detection of an Extrasolar Planet Atmosphere. ApJ568, 377–384.
Christensen-Dalsgaard, J., Dappen, W., Ajukov, S. V., Anderson, E. R., Antia, H. M., Basu, S., Baturin, V. A., Berthomieu, G., Chaboyer, B., Chitre, S. M., Cox, A. N., Demarque, P., Donatowicz, J., Dziembowski, W. A., Gabriel, M., Gough, D. O., Guenther, D. B., Guzik, J. A., Harvey, J. W., Hill, F., Houdek, G., Iglesias, C. A., Kosovichev, A. G., Leibacher, J. W., Morel, P., Proffitt, C. R., Provost, J., Reiter, J., Rhodes, Jr., E. J., Rogers, F. J., Roxburgh, I. W., Thompson, M. J., Ulrich, R. K., May 1996. The Current State of Solar Modeling. Science 272, 1286–1292.
Cohen, E. R., Taylor, B. N., 1987. The 1986 adjustment of the fundamental physical constants. Reviews of Modern Physics 59, 1121–1148.
Collins, G. W., da Silva, L. B., Celliers, P., Gold, D. M., Foord, M. E., Wallace, R. J., Ng, A., Weber, S. V., Budil, K. S., Cauble, R., Aug. 1998. Measurements of the equation of state of deuterium at the fluid insulator-metal transition. Science 281, 1178–1181.
Connerney, J. E. P., Ness, N. F., Acuna, M. H., Jul. 1982. Zonal harmonic model of Saturn's magnetic field from Voyager 1 and 2 observations. Nature298, 44–46.
Conrath, B., Hanel, R., Gautier, D., Marten, A., Lindal, G., Dec. 1987. The helium abundance of Uranus from Voyager measurements. JGR92, 15003–15010.
Conrath, B. J., Gautier, D., Mar. 2000. Saturn Helium Abundance: A Reanalysis of Voyager Measurements. Icarus144, 124–134.
Conrath, B. J., Gautier, D., Lindal, G. F., Samuelson, R. E., Shaffer, W. A., Oct. 1991. The helium abundance of Neptune from Voyager measurements. JGR96, 18907.
Cooper, C. S., Showman, A. P., Aug. 2005. Dynamic Meteorology at the Photosphere of HD 209458b. ApJL629, L45–L48.
Crossfield, I. J. M., Barman, T., Hansen, B. M. S., Tanaka, I., Kodama, T., Dec. 2012. Re-evaluating WASP-12b: Strong Emission at 2.315 μm, Deeper Occultations, and an Isothermal Atmosphere. ApJ760, 140.

Crouzet, N., McCullough, P. R., Burke, C., Long, D., Dec. 2012. Transmission Spectroscopy of Exoplanet XO-2b Observed with Hubble Space Telescope NICMOS. ApJ761, 7.

da Silva, L. B., Celliers, P., Collins, G. W., Budil, K. S., Holmes, N. C., Barbee, Jr., T. W., Hammel, B. A., Kilkenny, J. D., Wallace, R. J., Ross, M., Cauble, R., Ng, A., Chiu, G., Jan. 1997. Absolute Equation of State Measurements on Shocked Liquid Deuterium up to 200 GPa (2 Mbar). Physical Review Letters 78, 483–486.

Davies, M. E., Abalakin, V. K., Bursa, M., Lederle, T., Lieske, J. H., May 1986. Report of the IAU/IAG/COSPAR working group on cartographic coordinates and rotational elements of the planets and satellites - 1985. Celestial Mechanics 39, 103–113.

de Pater, I., Romani, P. N., Atreya, S. K., Jun. 1991. Possible microwave absorption by H2S gas in Uranus' and Neptune's atmospheres. Icarus91, 220–233.

de Pater, I., Sromovsky, L. A., Hammel, H. B., Fry, P. M., LeBeau, R. P., Rages, K., Showalter, M., Matthews, K., Sep. 2011. Post-equinox observations of Uranus: Berg's evolution, vertical structure, and track towards the equator. Icarus215, 332–345.

Deleuil, M., Bonomo, A. S., Ferraz-Mello, S., Erikson, A., Bouchy, F., Havel, M., Aigrain, S., Almenara, J.-M., Alonso, R., Auvergne, M., Baglin, A., Barge, P., Bordé, P., Bruntt, H., Cabrera, J., Carpano, S., Cavarroc, C., Csizmadia, S., Damiani, C., Deeg, H. J., Dvorak, R., Fridlund, M., Hébrard, G., Gandolfi, D., Gillon, M., Guenther, E., Guillot, T., Hatzes, A., Jorda, L., Léger, A., Lammer, H., Mazeh, T., Moutou, C., Ollivier, M., Ofir, A., Parviainen, H., Queloz, D., Rauer, H., Rodríguez, A., Rouan, D., Santerne, A., Schneider, J., Tal-Or, L., Tingley, B., Weingrill, J., Wuchterl, G., Feb. 2012. Transiting exoplanets from the CoRoT space mission. XX. CoRoT-20b: A very high density, high eccentricity transiting giant planet. A&A538, A145.

Deming, D., Wilkins, A., McCullough, P., Burrows, A., Fortney, J. J., Agol, E., Dobbs-Dixon, I., Madhusudhan, N., Crouzet, N., Desert, J.-M., Gilliland, R. L., Haynes, K., Knutson, H. A., Line, M., Magic, Z., Mandell, A. M., Ranjan, S., Charbonneau, D., Clampin, M., Seager, S., Showman, A. P., Sep. 2013. Infrared Transmission Spectroscopy of the Exoplanets HD 209458b and XO-1b Using the Wide Field Camera-3 on the Hubble Space Telescope. ApJ774, 95.

Désert, J.-M., Lecavelier des Etangs, A., Hébrard, G., Sing, D. K., Ehrenreich, D., Ferlet, R., Vidal-Madjar, A., Jul. 2009. Search for Carbon Monoxide in the Atmosphere of the Transiting Exoplanet HD 189733b. ApJ699, 478–485.

Desjarlais, M. P., Aug. 2003. Density-functional calculations of the liquid deuterium Hugoniot, reshock, and reverberation timing. Phys. Rev. B68 (6), 064204–+.

Fegley, B. J., Lodders, K., Jul. 1994. Chemical models of the deep atmospheres of Jupiter and Saturn. Icarus 110, 117–154.

Feuchtgruber, H., Lellouch, E., Orton, G., de Graauw, T., Vandenbussche, B., Swinyard, B., Moreno, R., Jarchow, C., Billebaud, F., Cavalié, T., Sidher, S., Hartogh, P., Mar. 2013. The D/H ratio in the atmospheres of Uranus and Neptune from Herschel-PACS observations. A&A551, A126.

Fischer, D. A., Valenti, J., Apr. 2005. The Planet-Metallicity Correlation. ApJ622, 1102–1117.

Fletcher, L. N., Baines, K. H., Momary, T. W., Showman, A. P., Irwin, P. G. J., Orton, G. S., Roos-Serote, M., Merlet, C., Aug. 2011. Saturn's tropospheric composition and clouds from Cassini/VIMS 4.6-5.1 μm nightside spectroscopy. Icarus214, 510–533.

Fletcher, L. N., Orton, G. S., Teanby, N. A., Irwin, P. G. J., Aug. 2009a. Phosphine on Jupiter and Saturn from Cassini/CIRS. Icarus202, 543–564.

Fletcher, L. N., Orton, G. S., Teanby, N. A., Irwin, P. G. J., Bjoraker, G. L., Feb. 2009b. Methane and its isotopologues on Saturn from Cassini/CIRS observations. Icarus199, 351–367.

Fortney, J. J., Hubbard, W. B., Jul. 2003. Phase separation in giant planets: inhomogeneous evolution of Saturn. Icarus 164, 228–243.

Fortney, J. J., Ikoma, M., Nettelmann, N., Guillot, T., Marley, M. S., Mar. 2011. Self-consistent Model Atmospheres and the Cooling of the Solar System's Giant Planets. ApJ729, 32.

Fortney, J. J., Nettelmann, N., May 2010. The Interior Structure, Composition, and Evolution of Giant Planets. Space Sci. Rev.152, 423–447.

Fortney, J. J., Saumon, D., Marley, M. S., Lodders, K., Freedman, R. S., May 2006. Atmosphere, Interior, and Evolution of the Metal-rich Transiting Planet HD 149026b. ApJ642, 495–504.

Fortov, V. E., Ilkaev, R. I., Arinin, V. A., Burtzev, V. V., Golubev, V. A., Iosilevskiy, I. L., Khrustalev, V. V., Mikhailov, A. L., Mochalov, M. A., Ternovoi, V. Y., Zhernokletov, M. V., Nov. 2007. Phase Transition in a Strongly Nonideal Deuterium Plasma Generated by Quasi-Isentropical Compression at Megabar Pressures. Physical Review Letters 99 (18), 185001.

Fossati, L., Haswell, C. A., Froning, C. S., Hebb, L., Holmes, S., Kolb, U., Helling, C., Carter, A., Wheatley, P., Collier Cameron, A., Loeillet, B., Pollacco, D., Street, R., Stempels, H. C., Simpson, E., Udry, S., Joshi, Y. C., West, R. G., Skillen, I., Wilson, D., May 2010. Metals in the Exosphere of the Highly Irradiated Planet WASP-12b. ApJL714, L222–L227.

Freedman, R. S., Marley, M. S., Lodders, K., Feb. 2008. Line and Mean Opacities for Ultracool Dwarfs and Extrasolar Planets. ApJS174, 504–513.

French, M., Becker, A., Lorenzen, W., Nettelmann, N., Bethkenhagen, M., Wicht, J., Redmer, R., Sep. 2012. Ab Initio Simulations for Material Properties along the Jupiter Adiabat. ApJS202, 5.

French, M., Mattsson, T. R., Nettelmann, N., Redmer, R., Feb. 2009. Equation of state and phase diagram of water at ultrahigh pressures as in planetary interiors. Phys. Rev. B79 (5), 054107.

Gastine, T., Wicht, J., Aurnou, J. M., Jul. 2013. Zonal flow regimes in rotating anelastic spherical shells: An application to giant planets. Icarus225, 156–172.

Gaulme, P., Schmider, F.-X., Gay, J., Guillot, T., Jacob, C., Jul. 2011. Detection of Jovian seismic waves: a new probe of its interior structure. A&A531, A104.

Gautier, D., Conrath, B. J., Owen, T., De Pater, I., Atreya, S. K., 1995. The Troposphere of Neptune. Neptune and Triton, UofA Press, pp. 547–611.

Gautier, D., Hersant, F., Mousis, O., Lunine, J. I., Oct. 2001. Erratum: Enrichments in Volatiles in Jupiter: A New Interpretation of the Galileo Measurements. ApJL559, L183–L183.

Giampieri, G., Dougherty, M. K., Smith, E. J., Russell, C. T., May 2006. A regular period for Saturn's magnetic field that may track its internal rotation. Nature441, 62–64.

Gibson, N. P., Pont, F., Aigrain, S., Mar. 2011. A new look at NICMOS transmission spectroscopy of HD 189733, GJ-436 and XO-1: no conclusive evidence for molecular features. MNRAS411, 2199–2213.

Gierasch, P. J., Ingersoll, A. P., Banfield, D., Ewald, S. P., Helfenstein, P., Simon-Miller, A., Vasavada, A., Breneman, H. H., Senske, D. A., A4 Galileo Imaging Team, Feb. 2000. Observation of moist convection in Jupiter's atmosphere. Nature403, 628–630.

Glatzmaier, G., Evonuk, M., Rogers, T., Feb. 2009. Differential rotation in giant planets maintained by density-stratified turbulent convection. Geophysical and Astrophysical Fluid Dynamics 103, 31–51.
Gonzalez, G., Jun. 1998. Spectroscopic analyses of the parent stars of extrasolar planetary system candidates. A&A334, 221–238.
Goukenleuque, C., Bézard, B., Joguet, B., Lellouch, E., Freedman, R., Feb. 2000. A Radiative Equilibrium Model of 51 Peg b. Icarus 143, 308–323.
Guervilly, C., Cardin, P., Schaeffer, N., Mar. 2012. A dynamo driven by zonal jets at the upper surface: Applications to giant planets. Icarus218, 100–114.
Guillot, T., Oct. 1999a. A comparison of the interiors of Jupiter and Saturn. Plan. Space Sci.47, 1183–1200.
Guillot, T., Oct. 1999b. Interior of Giant Planets Inside and Outside the Solar System. Science 286, 72–77.
Guillot, T., Jan. 2005. THE INTERIORS OF GIANT PLANETS: Models and Outstanding Questions. Annual Review of Earth and Planetary Sciences 33, 493–530.
Guillot, T., Aug. 2008. The composition of transiting giant extrasolar planets. Physica Scripta Volume T 130 (1), 014023.
Guillot, T., Sep. 2010. On the radiative equilibrium of irradiated planetary atmospheres. A&A520, A27.
Guillot, T., Burrows, A., Hubbard, W. B., Lunine, J. I., Saumon, D., Mar. 1996. Giant Planets at Small Orbital Distances. ApJL459, L35–L39.
Guillot, T., Hueso, R., Mar. 2006. The composition of Jupiter: sign of a (relatively) late formation in a chemically evolved protosolar disc. MNRAS367, L47–L51.
Guillot, T., Santos, N. C., Pont, F., Iro, N., Melo, C., Ribas, I., Jul. 2006. A correlation between the heavy element content of transiting extrasolar planets and the metallicity of their parent stars. A&A453, L21–L24.
Guillot, T., Showman, A. P., Apr. 2002. Evolution of "51 pegasus b-like" planets. A&A385, 156–165.
Guillot, T., Stevenson, D. J., Hubbard, W. B., Saumon, D., 2004. The interior of Jupiter. Jupiter. The Planet, Satellites and Magnetosphere, pp. 35–57.
Gulkis, S., Janssen, M. A., Olsen, E. T., Apr. 1978. Evidence for the depletion of ammonia in the Uranus atmosphere. Icarus 34, 10–19.
Gurnett, D. A., Kurth, W. S., Hospodarsky, G. B., Persoon, A. M., Averkamp, T. F., Cecconi, B., Lecacheux, A., Zarka, P., Canu, P., Cornilleau-Wehrlin, N., Galopeau, P., Roux, A., Harvey, C., Louarn, P., Bostrom, R., Gustafsson, G., Wahlund, J.-E., Desch, M. D., Farrell, W. M., Kaiser, M. L., Goetz, K., Kellogg, P. J., Fischer, G., Ladreiter, H.-P., Rucker, H., Alleyne, H., Pedersen, A., Feb. 2005. Radio and Plasma Wave Observations at Saturn from Cassini's Approach and First Orbit. Science 307, 1255–1259.
Hammel, H. B., de Pater, I., Gibbard, S. G., Lockwood, G. W., Rages, K., May 2005. New cloud activity on Uranus in 2004: First detection of a southern feature at 2.2 μm. Icarus 175, 284–288.
Hansen, B. M. S., Dec. 2008. On the Absorption and Redistribution of Energy in Irradiated Planets. ApJS179, 484–508.
Harrington, J., Hansen, B. M., Luszcz, S. H., Seager, S., Deming, D., Menou, K., Cho, J. Y.-K., Richardson, L. J., Oct. 2006. The Phase-Dependent Infrared Brightness of the Extrasolar Planet υ Andromedae b. Science 314, 623–626.
Hedman, M. M., Nicholson, P. D., Jul. 2013. Kronoseismology: Using Density Waves in Saturn's C Ring to Probe the Planet's Interior. AJ146, 12.
Heimpel, M., Gómez Pérez, N., Jul. 2011. On the relationship between zonal jets and dynamo action in giant planets. Geophys. Res. Let.38, 14201.
Helled, R., Jul. 2011. Constraining Saturn's Core Properties by a Measurement of Its Moment of Inertia – Implications to the Cassini Solstice Mission. ApJL735, L16.
Helled, R., Anderson, J. D., Podolak, M., Schubert, G., Jan. 2011a. Interior Models of Uranus and Neptune. ApJ726, 15.
Helled, R., Anderson, J. D., Schubert, G., Nov. 2010. Uranus and Neptune: Shape and rotation. Icarus210, 446–454.
Helled, R., Anderson, J. D., Schubert, G., Stevenson, D. J., Dec. 2011b. Jupiter's moment of inertia: A possible determination by Juno. Icarus216, 440–448.
Helled, R., Bodenheimer, P., Feb. 2011. The effects of metallicity and grain growth and settling on the early evolution of gaseous protoplanets. Icarus211, 939–947.
Helled, R., Guillot, T., Apr. 2013. Interior Models of Saturn: Including the Uncertainties in Shape and Rotation. ApJ767, 113.
Hersant, F., Gautier, D., Lunine, J. I., Jun. 2004. Enrichment in volatiles in the giant planets of the Solar System. Plan. Space Sci.52, 623–641.
Hicks, D. G., Boehly, T. R., Celliers, P. M., Eggert, J. H., Moon, S. J., Meyerhofer, D. D., Collins, G. W., Jan. 2009. Laser-driven single shock compression of fluid deuterium from 45 to 220 GPa. Phys. Rev. B79 (1), 014112.
Hubbard, W. B., Jun. 1968. Thermal structure of Jupiter. ApJ152, 745–754.
Hubbard, W. B., Feb. 1977. The Jovian surface condition and cooling rate. Icarus 30, 305–310.
Hubbard, W. B., 1989. Structure and composition of giant planet interiors. Origin and Evolution of Planetary and Satellite Atmospheres, pp. 539–563.
Hubbard, W. B., Feb. 1999. NOTE: Gravitational Signature of Jupiter's Deep Zonal Flows. Icarus137, 357–359.
Hubbard, W. B., May 2013. Concentric Maclaurin Spheroid Models of Rotating Liquid Planets. ApJ768, 43.
Hubbard, W. B., Guillot, T., Marley, M. S., Burrows, A., Lunine, J. I., Saumon, D. S., Oct. 1999. Comparative evolution of Jupiter and Saturn. Plan. Space Sci.47, 1175–1182.
Hubbard, W. B., Pearl, J. C., Podolak, M., Stevenson, D. J., 1995. The Interior of Neptune. Neptune and Triton, UofA Press, pp. 109–138.
Hueso, R., Sánchez-Lavega, A., Guillot, T., Oct. 2002. A model for large-scale convective storms in Jupiter. Journal of Geophysical Research (Planets) 107, 5–1.
Ida, S., Lin, D. N. C., Mar. 2004a. Toward a Deterministic Model of Planetary Formation. I. A Desert in the Mass and Semimajor Axis Distributions of Extrasolar Planets. ApJ604, 388–413.
Ida, S., Lin, D. N. C., Nov. 2004b. Toward a Deterministic Model of Planetary Formation. II. The Formation and Retention of Gas Giant Planets around Stars with a Range of Metallicities. ApJ616, 567–572.
Ikoma, M., Guillot, T., Genda, H., Tanigawa, T., Ida, S., Oct. 2006. On the Origin of HD 149026b. ApJ650, 1150–1159.
Ingersoll, A. P., Barnet, C. D., Beebe, R. F., Flasar, F. M., Hinson, D. P., Limaye, S. S., Sromovsky, L. A., Suomi, V. E., 1995. Dynamic Meteorology of Neptune. Neptune and Triton, UofA Press, pp. 613–682.
Iorio, L., Aug. 2010. Juno, the angular momentum of Jupiter and the Lense-Thirring effect. New Astronomy 15, 554–560.
Iro, N., Bézard, B., Guillot, T., Jun. 2005. A time-dependent radiative model of HD 209458b. A&A436, 719–727.
Irwin, P. G. J., Lellouch, E., de Bergh, C., Courtin, R., Bézard, B., Fletcher, L. N., Orton, G. S., Teanby, N. A., Calcutt, S. B., Tice, D., Hurley, J.,

Davis, G. R., Jan. 2014. Line-by-line analysis of Neptune's near-IR spectrum observed with Gemini/NIFS and VLT/CRIRES. Icarus227, 37–48.
Jackiewicz, J., Nettelmann, N., Marley, M., Fortney, J., Aug. 2012. Forward and inverse modeling for jovian seismology. Icarus220, 844–854.
Jacobson, R. A., May 2009. The Orbits of the Neptunian Satellites and the Orientation of the Pole of Neptune. AJ137, 4322–4329.
Jacobson, R. A., Antreasian, P. G., Bordi, J. J., Criddle, K. E., Ionasescu, R., Jones, J. B., Mackenzie, R. A., Meek, M. C., Parcher, D., Pelletier, F. J., Owen, Jr., W. M., Roth, D. C., Roundhill, I. M., Stauch, J. R., Dec. 2006. The Gravity Field of the Saturnian System from Satellite Observations and Spacecraft Tracking Data. AJ132, 2520–2526.
Karkoschka, E., Tomasko, M. G., Jan. 2011. The haze and methane distributions on Neptune from HST-STIS spectroscopy. Icarus211, 780–797.
Kaspi, Y., Showman, A. P., Hubbard, W. B., Aharonson, O., Helled, R., May 2013. Atmospheric confinement of jet streams on Uranus and Neptune. Nature497, 344–347.
Kippenhahn, R., Weigert, A., 1994. Stellar Structure and Evolution. Stellar Structure and Evolution, XVI, 468 pp. 192 figs.. Springer-Verlag Berlin Heidelberg New York. Also Astronomy and Astrophysics Library.
Knudson, M. D., Desjarlais, M. P., Nov. 2009. Shock Compression of Quartz to 1.6 TPa: Redefining a Pressure Standard. Physical Review Letters 103 (22), 225501.
Knudson, M. D., Desjarlais, M. P., Lemke, R. W., Mattsson, T. R., French, M., Nettelmann, N., Redmer, R., Mar. 2012. Probing the Interiors of the Ice Giants: Shock Compression of Water to 700 GPa and 3.8g/cm^3. Physical Review Letters 108 (9), 091102.
Knudson, M. D., Hanson, D. L., Bailey, J. E., Hall, C. A., Asay, J. R., Deeney, C., Apr. 2004. Principal Hugoniot, reverberating wave, and mechanical reshock measurements of liquid deuterium to 400 GPa using plate impact techniques. Phys. Rev. B69 (14), 144209–+.
Knutson, H. A., Charbonneau, D., Allen, L. E., Fortney, J. J., Agol, E., Cowan, N. B., Showman, A. P., Cooper, C. S., Megeath, S. T., May 2007. A map of the day-night contrast of the extrasolar planet HD 189733b. Nature447, 183–186.
Kramm, U., Nettelmann, N., Fortney, J. J., Neuhäuser, R., Redmer, R., Feb. 2012. Constraining the interior of extrasolar giant planets with the tidal Love number k_2 using the example of HAT-P-13b. A&A538, A146.
Kuchner, M. J., Oct. 2003. Volatile-rich Earth-Mass Planets in the Habitable Zone. ApJL596, L105–L108.
Kunde, V., Hanel, R., Maguire, W., Gautier, D., Baluteau, J. P., Marten, A., Chedin, A., Husson, N., Scott, N., Dec. 1982. The tropospheric gas composition of Jupiter's north equatorial belt /NH3, PH3, CH3D, GeH4, H2O/ and the Jovian D/H isotopic ratio. ApJ263, 443–467.
Lammer, H., Selsis, F., Ribas, I., Guinan, E. F., Bauer, S. J., Weiss, W. W., Dec. 2003. Atmospheric Loss of Exoplanets Resulting from Stellar X-Ray and Extreme-Ultraviolet Heating. ApJL598, L121–L124.
Laughlin, G., Crismani, M., Adams, F. C., Mar. 2011. On the Anomalous Radii of the Transiting Extrasolar Planets. ApJL729, L7.
Leconte, J., Chabrier, G., Apr. 2012. A new vision of giant planet interiors: Impact of double diffusive convection. A&A540, A20.
Leconte, J., Chabrier, G., Baraffe, I., Levrard, B., Jun. 2010. Is tidal heating sufficient to explain bloated exoplanets? Consistent calculations accounting for finite initial eccentricity. A&A516, A64.
Léger, A., Selsis, F., Sotin, C., Guillot, T., Despois, D., Mawet, D., Ollivier, M., Labèque, A., Valette, C., Brachet, F., Chazelas, B., Lammer, H., Jun. 2004. A new family of planets? "Ocean-Planets". Icarus 169, 499–504.
Lellouch, E., Bézard, B., Fouchet, T., Feuchtgruber, H., Encrenaz, T., de Graauw, T., May 2001. The deuterium abundance in Jupiter and Saturn from ISO-SWS observations. A&A370, 610–622.
Levrard, B., Correia, A. C. M., Chabrier, G., Baraffe, I., Selsis, F., Laskar, J., Jan. 2007. Tidal dissipation within hot Jupiters: a new appraisal. A&A462, L5–L8.
Lian, Y., Showman, A. P., May 2010. Generation of equatorial jets by large-scale latent heating on the giant planets. Icarus207, 373–393.
Lindal, G. F., Mar. 1992a. The atmosphere of Neptune - an analysis of radio occultation data acquired with Voyager 2. AJ103, 967–982.
Lindal, G. F., Mar. 1992b. The atmosphere of Neptune - an analysis of radio occultation data acquired with Voyager 2. AJ103, 967–982.
Lindal, G. F., Sweetnam, D. N., Eshleman, V. R., Jun. 1985. The atmosphere of Saturn - an analysis of the Voyager radio occultation measurements. AJ90, 1136–1146.
Lindal, G. F., Wood, G. E., Levy, G. S., Anderson, J. D., Sweetnam, D. N., Hotz, H. B., Buckles, B. J., Holmes, D. P., Doms, P. E., Eshleman, V. R., Tyler, G. L., Croft, T. A., Sep. 1981. The atmosphere of Jupiter - an analysis of the Voyager radio occultation measurements. JGR86, 8721–8727.
Little, B., Anger, C. D., Ingersoll, A. P., Vasavada, A. R., Senske, D. A., Breneman, H. H., Borucki, W. J., The Galileo SSI Team, Dec. 1999. Galileo Images of Lightning on Jupiter. Icarus 142, 306–323.
Liu, J., Schneider, T., Nov. 2011. Convective Generation of Equatorial Superrotation in Planetary Atmospheres. Journal of Atmospheric Sciences 68, 2742–2756.
Liu, J., Schneider, T., Kaspi, Y., May 2013. Predictions of thermal and gravitational signals of Jupiter's deep zonal winds. Icarus224, 114–125.
Lodders, K., Feb. 2008. The Solar Argon Abundance. ApJ674, 607–611.
Lodders, K., Fegley, Jr., B., Dec. 1994. The origin of carbon monoxide in Neptunes's atmosphere. Icarus 112, 368–375.
Lodders, K., Palme, H., Gail, H.-P., 2009. Abundances of the Elements in the Solar System. Landolt Börnstein, 44.
Lopez, E. D., Fortney, J. J., Miller, N., Dec. 2012. How Thermal Evolution and Mass-loss Sculpt Populations of Super-Earths and Sub-Neptunes: Application to the Kepler-11 System and Beyond. ApJ761, 59.
Lorenzen, W., Holst, B., Redmer, R., Dec. 2011. Metallization in hydrogen-helium mixtures. Phys. Rev. B84 (23), 235109.
Loubeyre, P., Brygoo, S., Eggert, J., Celliers, P. M., Spaulding, D. K., Rygg, J. R., Boehly, T. R., Collins, G. W., Jeanloz, R., Oct. 2012. Extended data set for the equation of state of warm dense hydrogen isotopes. Phys. Rev. B86 (14), 144115.
Loubeyre, P., Letoullec, R., Pinceaux, J. P., May 1991. A new determination of the binary phase diagram of H_2-He mixtures at 296 K. Journal of Physics Condensed Matter 3, 3183–3192.
Mardling, R. A., Sep. 2010. The determination of planetary structure in tidally relaxed inclined systems. MNRAS407, 1048–1069.
Marley, M. S., Fortney, J. J., Hubickyj, O., Bodenheimer, P., Lissauer, J. J., Sep. 2006. On the Luminosity of Young Jupiters. ArXiv Astrophysics e-prints.
Marley, M. S., Gómez, P., Podolak, M., Nov. 1995. Monte Carlo interior models for Uranus and Neptune. JGR100, 23349–23354.
Marley, M. S., Porco, C. C., Dec. 1993. Planetary acoustic mode seismology - Saturn's rings. Icarus106, 508.
Marley, M. S., Saumon, D., Guillot, T., Freedman, R. S., Hubbard, W. B., Burrows, A., Lunine, J. I., Jun. 1996. Atmospheric, Evolutionary, and

Spectral Models of the Brown Dwarf Gliese 229 B. Science 272, 1919–1921.
Marty, B., Chaussidon, M., Wiens, R. C., Jurewicz, A. J. G., Burnett, D. S., Jun. 2011. A ^{15}N-Poor Isotopic Composition for the Solar System As Shown by Genesis Solar Wind Samples. Science 332, 1533–.
Marty, B., Guillot, T., Coustenis, A., Achilleos, N., Alibert, Y., Asmar, S., Atkinson, D., Atreya, S., Babasides, G., Baines, K., Balint, T., Banfield, D., Barber, S., Bézard, B., Bjoraker, G. L., Blanc, M., Bolton, S., Chanover, N., Charnoz, S., Chassefière, E., Colwell, J. E., Deangelis, E., Dougherty, M., Drossart, P., Flasar, F. M., Fouchet, T., Frampton, R., Franchi, I., Gautier, D., Gurvits, L., Hueso, R., Kazeminejad, B., Krimigis, T., Jambon, A., Jones, G., Langevin, Y., Leese, M., Lellouch, E., Lunine, J., Milillo, A., Mahaffy, P., Mauk, B., Morse, A., Moreira, M., Moussas, X., Murray, C., Mueller-Wodarg, I., Owen, T. C., Pogrebenko, S., Prangé, R., Read, P., Sanchez-Lavega, A., Sarda, P., Stam, D., Tinetti, G., Zarka, P., Zarnecki, J., Mar. 2009. Kronos: exploring the depths of Saturn with probes and remote sensing through an international mission. Experimental Astronomy 23, 947–976.
Mayor, M., Queloz, D., Nov. 1995. A Jupiter-Mass Companion to a Solar-Type Star. Nature378, 355–+.
McMahon, J. M., Morales, M. A., Pierleoni, C., Ceperley, D. M., Oct. 2012. The properties of hydrogen and helium under extreme conditions. Reviews of Modern Physics 84, 1607–1653.
Militzer, B., Ceperley, D. M., Kress, J. D., Johnson, J. D., Collins, L. A., Mazevet, S., Dec. 2001. Calculation of a Deuterium Double Shock Hugoniot from Ab Initio Simulations. Physical Review Letters 87 (26), A265502+.
Militzer, B., Hubbard, W. B., Sep. 2013. Ab Initio Equation of State for Hydrogen-Helium Mixtures with Recalibration of the Giant-planet Mass-Radius Relation. ApJ774, 148.
Militzer, B., Hubbard, W. B., Vorberger, J., Tamblyn, I., Bonev, S. A., Nov. 2008. A Massive Core in Jupiter Predicted from First-Principles Simulations. ApJL688, L45–L48.
Miller, N., Fortney, J. J., Aug. 2011. The Heavy-element Masses of Extrasolar Giant Planets, Revealed. ApJL736, L29.
Mochalov, M. A., Il'kaev, R. I., Fortov, V. E., Mikhailov, A. L., Makarov, Y. M., Arinin, V. A., Blikov, A. O., Baurin, A. Y., Komrakov, V. A., Ogorodnikov, V. A., Ryzhkov, A. V., Pronin, E. A., Yukhimchuk, A. A., Oct. 2012. Measurement of quasi-isentropic compressibility of helium and deuterium at pressures of 1500-2000 GPa. Soviet Journal of Experimental and Theoretical Physics 115, 614–625.
Moorhead, A. V., Adams, F. C., Nov. 2005. Giant planet migration through the action of disk torques and planet planet scattering. Icarus 178, 517–539.
Morales, M. A., Hamel, S., Caspersen, K., Schwegler, E., May 2013a. Hydrogen-helium demixing from first principles: From diamond anvil cells to planetary interiors. Phys. Rev. B87 (17), 174105.
Morales, M. A., McMahon, J. M., Pierleoni, C., Ceperley, D. M., Feb. 2013b. Nuclear Quantum Effects and Nonlocal Exchange-Correlation Functionals Applied to Liquid Hydrogen at High Pressure. Physical Review Letters 110 (6), 065702.
Morales, M. A., Pierleoni, C., Ceperley, D. M., Feb. 2010. Equation of state of metallic hydrogen from coupled electron-ion Monte Carlo simulations. Phys. Rev. E81 (2), 021202.
Morales, M. A., Schwegler, E., Ceperley, D., Pierleoni, C., Hamel, S., Caspersen, K., Feb. 2009. Phase separation in hydrogen-helium mixtures at Mbar pressures. Proceedings of the National Academy of Science 106, 1324.
Mordasini, C., Oct. 2013. Luminosity of young Jupiters revisited. Massive cores make hot planets. A&A558, A113.
Mordasini, C., Alibert, Y., Georgy, C., Dittkrist, K.-M., Klahr, H., Henning, T., Nov. 2012. Characterization of exoplanets from their formation. II. The planetary mass-radius relationship. A&A547, A112.
Mousis, O., Lunine, J. I., Madhusudhan, N., Johnson, T. V., May 2012. Nebular Water Depletion as the Cause of Jupiter's Low Oxygen Abundance. ApJL751, L7.
Moutou, C., Deleuil, M., Guillot, T., Baglin, A., Bordé, P., Bouchy, F., Cabrera, J., Csizmadia, S., Deeg, H. J., Nov. 2013. CoRoT: Harvest of the exoplanet program. Icarus226, 1625–1634.
Ness, N. F., Acuna, M. H., Behannon, K. W., Burlaga, L. F., Connerney, J. E. P., Lepping, R. P., Jul. 1986. Magnetic fields at Uranus. Science 233, 85–89.
Ness, N. F., Acuna, M. H., Burlaga, L. F., Connerney, J. E. P., Lepping, R. P., Dec. 1989. Magnetic fields at Neptune. Science 246, 1473–1478.
Nettelmann, N., Becker, A., Holst, B., Redmer, R., May 2012. Jupiter Models with Improved Ab Initio Hydrogen Equation of State (H-REOS.2). ApJ750, 52.
Nettelmann, N., Helled, R., Fortney, J. J., Redmer, R., Mar. 2013a. New indication for a dichotomy in the interior structure of Uranus and Neptune from the application of modified shape and rotation data. Plan. Space Sci.77, 143–151.
Nettelmann, N., Püstow, R., Redmer, R., Jul. 2013b. Saturn layered structure and homogeneous evolution models with different EOSs. Icarus225, 548–557.
Noll, K. S., Larson, H. P., Jan. 1991. The spectrum of Saturn from 1990 to 2230/cm - Abundances of AsH3, CH3D, CO, GeH4, NH3, and PH3. Icarus89, 168–189.
Noll, K. S., Larson, H. P., Geballe, T. R., Feb. 1990. The abundance of AsH3 in Jupiter. Icarus83, 494–499.
Owen, T., Mahaffy, P., Niemann, H. B., Atreya, S., Donahue, T., Bar-Nun, A., de Pater, I., Nov. 1999. A low-temperature origin for the planetesimals that formed Jupiter. Nature402, 269–270.
Parmentier, V., Guillot, T., Feb. 2014. A non-grey analytical model for irradiated atmospheres. I: Derivation. A&A, in press.
Parmentier, V., Showman, A. P., Lian, Y., Oct. 2013. 3D mixing in hot Jupiters atmospheres. I. Application to the day/night cold trap in HD 209458b. A&A558, A91.
Pearl, J. C., Conrath, B. J., Oct. 1991. The albedo, effective temperature, and energy balance of Neptune, as determined from Voyager data. JGR96, 18921–+.
Podolak, M., Hubbard, W. B., Stevenson, D. J., 1991. Model of Uranus' interior and magnetic field. Uranus, UofA Press, pp. 29–61.
Podolak, M., Podolak, J. I., Marley, M. S., Feb. 2000. Further investigations of random models of Uranus and Neptune. Plan. Space Sci.48, 143–151.
Podolak, M., Weizman, A., Marley, M., Dec. 1995. Comparative models of Uranus and Neptune. Plan. Space Sci.43, 1517–1522.
Pont, F., Sing, D. K., Gibson, N. P., Aigrain, S., Henry, G., Husnoo, N., Jul. 2013. The prevalence of dust on the exoplanet HD 189733b from Hubble and Spitzer observations. MNRAS432, 2917–2944.

Rages, K., Hammel, H. B., Lockwood, G. W., Sep. 2002. A Prominent Apparition of Neptune's South Polar Feature. Icarus 159, 262–265.
Rauscher, E., Menou, K., Feb. 2013. Three-dimensional Atmospheric Circulation Models of HD 189733b and HD 209458b with Consistent Magnetic Drag and Ohmic Dissipation. ApJ764, 103.
Read, P. L., Dowling, T. E., Schubert, G., Jul. 2009. Saturn's rotation period from its atmospheric planetary-wave configuration. Nature460, 608–610.
Redmer, R., Mattsson, T. R., Nettelmann, N., French, M., Jan. 2011. The phase diagram of water and the magnetic fields of Uranus and Neptune. Icarus211, 798–803.
Ribas, I., Aug. 2006. Masses and Radii of Low-Mass Stars: Theory Versus Observations. Ap&SS304, 89–92.
Robinson, T. D., Catling, D. C., Jan. 2014. Common 0.1bar tropopause in thick atmospheres set by pressure-dependent infrared transparency. Nature Geoscience 7, 12–15.
Rosenblum, E., Garaud, P., Traxler, A., Stellmach, S., Apr. 2011. Turbulent Mixing and Layer Formation in Double-diffusive Convection: Three-dimensional Numerical Simulations and Theory. ApJ731, 66.
Rossow, W. B., Oct. 1978. Cloud microphysics - Analysis of the clouds of Earth, Venus, Mars, and Jupiter. Icarus36, 1–50.
Roulston, M. S., Stevenson, D. J., 1995. Prediction of neon depletion in Jupiter's atmosphere. In: EOS. Vol. 76. p. 343.
Russell, C. T., Dougherty, M. K., May 2010. Magnetic Fields of the Outer Planets. Space Sci. Rev.152, 251–269.
Salpeter, E. E., Apr. 1973. On Convection and Gravitational Layering in Jupiter and in Stars of Low Mass. ApJL181, L83+.
Sanchez-Lavega, A., Lecacheux, J., Gomez, J. M., Colas, F., Laques, P., Noll, K., Gilmore, D., Miyazaki, I., Parker, D., Feb. 1996. Large-scale storms in Saturn's atmosphere during 1994. Science 271, 631–634.
Sano, T., Ozaki, N., Sakaiya, T., Shigemori, K., Ikoma, M., Kimura, T., Miyanishi, K., Endo, T., Shiroshita, A., Takahashi, H., Jitsui, T., Hori, Y., Hironaka, Y., Iwamoto, A., Kadono, T., Nakai, M., Okuchi, T., Otani, K., Shimizu, K., Kondo, T., Kodama, R., Mima, K., Feb. 2011. Laser-shock compression and Hugoniot measurements of liquid hydrogen to 55 GPa. Phys. Rev. B83 (5), 054117.
Santos, N. C., Israelian, G., Mayor, M., Mar. 2004. Spectroscopic [Fe/H] for 98 extra-solar planet-host stars. Exploring the probability of planet formation. A&A415, 1153–1166.
Sato, B., Fischer, D. A., Henry, G. W., Laughlin, G., Butler, R. P., Marcy, G. W., Vogt, S. S., Bodenheimer, P., Ida, S., Toyota, E., Wolf, A., Valenti, J. A., Boyd, L. J., Johnson, J. A., Wright, J. T., Ammons, M., Robinson, S., Strader, J., McCarthy, C., Tah, K. L., Minniti, D., Nov. 2005. The N2K Consortium. II. A Transiting Hot Saturn around HD 149026 with a Large Dense Core. ApJ633, 465–473.
Saumon, D., Chabrier, G., van Horn, H. M., Aug. 1995. An Equation of State for Low-Mass Stars and Giant Planets. ApJS99, 713–+.
Saumon, D., Guillot, T., Jul. 2004. Shock Compression of Deuterium and the Interiors of Jupiter and Saturn. ApJ609, 1170–1180.
Saumon, D., Hubbard, W. B., Burrows, A., Guillot, T., Lunine, J. I., Chabrier, G., Apr. 1996. A Theory of Extrasolar Giant Planets. ApJ460, 993–+.
Schneider, J., Dedieu, C., Le Sidaner, P., Savalle, R., Zolotukhin, I., Aug. 2011. Defining and cataloging exoplanets: the exoplanet.eu database. A&A532, A79.
Schouten, J. A., de Kuijper, A., Michels, J. P. J., Oct. 1991. Critical line of He-H_2 up to 2500 K and the influence of attraction on fluid-fluid separation. Phys. Rev. B44, 6630–6634.
Seager, S., Deming, D., Sep. 2010. Exoplanet Atmospheres. Ann. Rev. Astron. Astrophys.48, 631–672.
Seager, S., Sasselov, D. D., Jul. 2000. Theoretical Transmission Spectra during Extrasolar Giant Planet Transits. ApJ537, 916–921.
Seiff, A., Kirk, D. B., Knight, T. C. D., Young, R. E., Mihalov, J. D., Young, L. A., Milos, F. S., Schubert, G., Blanchard, R. C., Atkinson, D., Sep. 1998. Thermal structure of Jupiter's atmosphere near the edge of a 5-μm hot spot in the north equatorial belt. JGR103, 22857–22890.
Showman, A. P., Guillot, T., Apr. 2002. Atmospheric circulation and tides of "51 Pegasus b-like" planets. A&A385, 166–180.
Showman, A. P., Ingersoll, A. P., Apr. 1998. Interpretation of Galileo Probe Data and Implications for Jupiter's Dry Downdrafts. Icarus 132, 205–220.
Showman, A. P., Kaspi, Y., Flierl, G. R., Feb. 2011. Scaling laws for convection and jet speeds in the giant planets. Icarus211, 1258–1273.
Simon-Miller, A. A., Gierasch, P. J., Beebe, R. F., Conrath, B., Flasar, F. M., Achterberg, R. K., the Cassini CIRS Team, Jul. 2002. New Observational Results Concerning Jupiter's Great Red Spot. Icarus 158, 249–266.
Sing, D. K., Désert, J.-M., Lecavelier Des Etangs, A., Ballester, G. E., Vidal-Madjar, A., Parmentier, V., Hebrard, G., Henry, G. W., Oct. 2009. Transit spectrophotometry of the exoplanet HD 189733b. I. Searching for water but finding haze with HST NICMOS. A&A505, 891–899.
Snellen, I. A. G., de Kok, R. J., de Mooij, E. J. W., Albrecht, S., Jun. 2010. The orbital motion, absolute mass and high-altitude winds of exoplanet HD209458b. Nature465, 1049–1051.
Soderlund, K. M., Heimpel, M. H., King, E. M., Aurnou, J. M., May 2013. Turbulent models of ice giant internal dynamics: Dynamos, heat transfer, and zonal flows. Icarus224, 97–113.
Spiegel, D. S., Burrows, A., Jul. 2013. Thermal Processes Governing Hot-Jupiter Radii. ApJ772, 76.
Spiegel, D. S., Silverio, K., Burrows, A., Jul. 2009. Can TiO Explain Thermal Inversions in the Upper Atmospheres of Irradiated Giant Planets? ApJ699, 1487–1500.
Spilker, L. J., Mar. 2012. Cassini: Science Highlights from the Equinox and Solstice Missions. In: Lunar and Planetary Institute Science Conference Abstracts. Vol. 43 of Lunar and Planetary Institute Science Conference Abstracts. p. 1358.
Sromovsky, L. A., Fry, P. M., Kim, J. H., Sep. 2011. Methane on Uranus: The case for a compact CH_4 cloud layer at low latitudes and a severe CH_4 depletion at high-latitudes based on re-analysis of Voyager occultation measurements and STIS spectroscopy. Icarus215, 292–312.
Stanley, S., Bloxham, J., Mar. 2004. Convective-region geometry as the cause of Uranus' and Neptune's unusual magnetic fields. Nature428, 151–153.
Stanley, S., Glatzmaier, G. A., May 2010. Dynamo Models for Planets Other Than Earth. Space Sci. Rev.152, 617–649.
Stevenson, D. J., 1982. Interiors of the giant planets. Annual Review of Earth and Planetary Sciences 10, 257–295.
Stevenson, D. J., May 1983. Planetary magnetic fields. Reports of Progress in Physics 46, 555–557.
Stevenson, D. J., Apr. 1985a. Cosmochemistry and structure of the giant planets and their satellites. Icarus 62, 4–15.
Stevenson, D. J., Apr. 1985b. Cosmochemistry and structure of the giant planets and their satellites. Icarus62, 4–15.
Stevenson, D. J., Salpeter, E. E., Oct. 1977a. The dynamics and helium distribution in hydrogen-helium fluid planets. ApJS35, 239–261.
Stevenson, D. J., Salpeter, E. E., Oct. 1977b. The phase diagram and transport properties for hydrogen-helium fluid planets. ApJS35, 221–237.

Sudarsky, D., Burrows, A., Hubeny, I., May 2003. Theoretical Spectra and Atmospheres of Extrasolar Giant Planets. ApJ588, 1121–1148.
Trafton, L. M., Feb. 1967. Model atmospheres of the major planets. ApJ147, 765–781.
Tsiganis, K., Gomes, R., Morbidelli, A., Levison, H. F., May 2005. Origin of the orbital architecture of the giant planets of the Solar System. Nature435, 459–461.
Vidal-Madjar, A., Huitson, C. M., Lecavelier Des Etangs, A., Sing, D. K., Ferlet, R., Désert, J.-M., Hébrard, G., Boisse, I., Ehrenreich, D., Moutou, C., Sep. 2011. The upper atmosphere of the exoplanet HD209458b revealed by the sodium D lines: temperature-pressure profile, ionization layer and thermosphere (Corrigendum). A&A533, C4.
Vidal-Madjar, A., Lecavelier des Etangs, A., Désert, J.-M., Ballester, G. E., Ferlet, R., Hébrard, G., Mayor, M., Mar. 2003. An extended upper atmosphere around the extrasolar planet HD209458b. Nature422, 143–146.
Visscher, C., Moses, J. I., Sep. 2011. Quenching of Carbon Monoxide and Methane in the Atmospheres of Cool Brown Dwarfs and Hot Jupiters. ApJ738, 72.
von Zahn, U., Hunten, D. M., Lehmacher, G., Sep. 1998a. Helium in Jupiter's atmosphere: Results from the Galileo probe helium interferometer experiment. JGR103, 22815–22830.
von Zahn, U., Hunten, D. M., Lehmacher, G., Sep. 1998b. Helium in Jupiter's atmosphere: Results from the Galileo probe helium interferometer experiment. JGR103, 22815–22830.
Vorberger, J., Tamblyn, I., Militzer, B., Bonev, S. A., Jan. 2007. Hydrogen-helium mixtures in the interiors of giant planets. Phys. Rev. B75 (2), 024206.
Vorontsov, S. V., Zharkov, V. N., Lubimov, V. M., Jan. 1976. The free oscillations of jupiter and saturn. Icarus27, 109–118.
Wahl, S. M., Wilson, H. F., Militzer, B., Aug. 2013. Solubility of Iron in Metallic Hydrogen and Stability of Dense Cores in Giant Planets. ApJ773, 95.
Warwick, J. W., Evans, D. R., Peltzer, G. R., Peltzer, R. G., Romig, J. H., Sawyer, C. B., Riddle, A. C., Schweitzer, A. E., Desch, M. D., Kaiser, M. L., Dec. 1989. Voyager planetary radio astronomy at Neptune. Science 246, 1498–1501.
Warwick, J. W., Evans, D. R., Romig, J. H., Sawyer, C. B., Desch, M. D., Kaiser, M. L., Alexander, J. K., Gulkis, S., Poynter, R. L., Jul. 1986. Voyager 2 radio observations of Uranus. Science 233, 102–106.
Weir, S. T., Mitchell, A. C., Nellis, W. J., Mar. 1996. Metallization of Fluid Molecular Hydrogen at 140 GPa (1.4 Mbar). Physical Review Letters 76, 1860–1863.
Wilson, H. F., Militzer, B., Mar. 2010. Sequestration of Noble Gases in Giant Planet Interiors. Physical Review Letters 104 (12), 121101.
Wilson, H. F., Militzer, B., Jan. 2012. Solubility of Water Ice in Metallic Hydrogen: Consequences for Core Erosion in Gas Giant Planets. ApJ745, 54.
Winn, J. N., Holman, M. J., Aug. 2005. Obliquity Tides on Hot Jupiters. ApJL628, L159–L162.
Wong, M. H., Mahaffy, P. R., Atreya, S. K., Niemann, H. B., Owen, T. C., Sep. 2004. Updated Galileo probe mass spectrometer measurements of carbon, oxygen, nitrogen, and sulfur on Jupiter. Icarus 171, 153–170.
Wright, J. T., Fakhouri, O., Marcy, G. W., Han, E., Feng, Y., Johnson, J. A., Howard, A. W., Fischer, D. A., Valenti, J. A., Anderson, J., Piskunov, N., Apr. 2011. The exoplanet orbit database. PASP123, 412–422.
Youdin, A. N., Mitchell, J. L., Oct. 2010. The Mechanical Greenhouse: Burial of Heat by Turbulence in Hot Jupiter Atmospheres. ApJ721, 1113–1126.
Zharkov, V. N., Trubitsyn, V. P., Feb. 1974. Internal constitution and the figures of the giant planets. Physics of the Earth and Planetary Interiors 8, 105–107.
Zharkov, V. N., Trubitsyn, V. P., 1978. Physics of planetary interiors. Astronomy and Astrophysics Series, Tucson: Pachart, 1978.